**ECOLE POLYTECHNIQUE FEDERALE DE LAUSANNE**
**SCHOOL OF LIFE SCIENCES**


Master project in Bioengineering

# CHARACTERIZATION OF THE AUDITORY SYSTEM RESPONSES TO INFRARED NEURAL STIMULATION OF THE COCHLEAR NUCLEUS

Carried out at the Eaton-Peabody Laboratory, Massachusetts Eye and Ear Infirmary and the Department of Otology and Laryngology, Harvard Medical School
Under the supervision of Prof. Daniel J. LEE

Done by

**AMELIE GUEX**

Under the direction of
PROF. Stéphanie LACOUR
In the Soft Bioelectronics Interfaces Laboratory
and
PROF. Olaf BLANKE
In the Laboratory of Cognitive Neuroscience

EPFL

External Expert:
Dr. Angélica PÉREZ FORNOS, Senior research associate, Centre romand d'implants cochléaires (CRIC), Geneva university hospital (HUG)

LAUSANNE, EPFL 2012

## Project summary

The aim of this project is to study the use of pulsed infrared laser light to stimulate the central auditory system. This novel approach may be a means to improve the efficacy of the current generation of electrically based Auditory Brainstem Implants (ABI).

Infrared neural stimulation (INS) has been shown to activate peripheral nerves and other excitable cells. This method appears to achieve a stimulation that is more spatially selective than traditional electrical methods. In this project, the use of INS as a means of activating the cochlear nucleus (CN) of a rodent model is investigated.

To characterize the response of the auditory system to INS of the CN, optically evoked auditory brainstem responses (ABR) as well as neurophysiologic multiunit recordings from the central nucleus of the inferior colliculus (IC) are obtained and analyzed. One aim of this project is studying the effects on the responses of different laser parameters, such as the pulse duration, the peak power, the laser wavelength and the stimulation pulse rate. A second aim is identifying the importance of the stimulation location on the surface of the CN in comparison with electrical stimulation. Finally, due to the known optophonic artifact generated by the infrared laser, the effect of deafening of the animals on the responses is studied.

The results show a successful activation of the auditory system of normal hearing animals, recorded both with ABR and IC recording techniques. The laser peak is the only parameters having a significant effect on the response. In deafened subjects, no significant responses can be recorded.

The conclusions of this study are that the optophonic effect predominates on the responses in hearing animals, and that INS alone is not a suitable technique for an ABI. Further work involves CN local responses measurements, as well as characterization of the cell types targeted by INS. Bimodal stimulation with combined INS and electrical stimulation is also a promising technique for the improvement of the ABI.

# Contents

# 1. Introduction and literature review

## 1.1. The Auditory System in Normal Hearing Individuals

As sound enters the external ear, the air pressure waves cause vibrations of the tympanic membrane. These vibrations are transmitted to the three ossicles of the middle ear: malleus, incus and stapes. The stapes vibrates against the oval window of the cochlea, transmitting the signal to the intracochlear fluids and the basilar membrane. Vibration of this membrane mechanically causes opening of ion channels at the tip of the inner hair cells, inducing depolarization. [2]

The hair cells, located along the basilar membrane, are mechanically stimulated by the fluid vibrations. This stimulation is tonotopic, with lower frequencies stimulating maximally the apical part of the cochlea and higher frequencies the basal region. This tonotopic organization is preserved throughout the auditory pathways (including the cochlear nucleus and inferior colliculus), finally terminating in the auditory cortex. [3]

Depolarization of the inner hair cells results in the release of neurotransmitter into the synaptic cleft found on the basilar end of the hair cell, resulting in the generation of an action potential that is propagated by the first order neuron of the auditory pathways, the spiral ganglion cells. These neurons give rise to the eighth cranial nerve called the vestibulocochlear nerve that terminates in the cochlear nucleus. The cochlear nucleus is the first relay station for all ascending sound information originating in the inner ear. Second order auditory neurons are found in the cochlear nuclei, with many projecting to the superior olive, on the contralateral side, and then to the lateral lemniscus and the inferior colliculus. Then, third order neurons project to the medial geniculate nucleus, in the thalamus, and these in turn to the primary auditory cortex. Many other auditory pathways are also involved, including a smaller ipsilateral side pathway going from the cochlear nucleus to the inferior colliculus via the lateral lemniscus. Descending pathways also play an important role in middle and inner ear function. Some of these involve auditory reflex pathways that function to 1) reduce the masking effects of background noise and 2) protect the inner ear when exposed to loud sounds. [2]

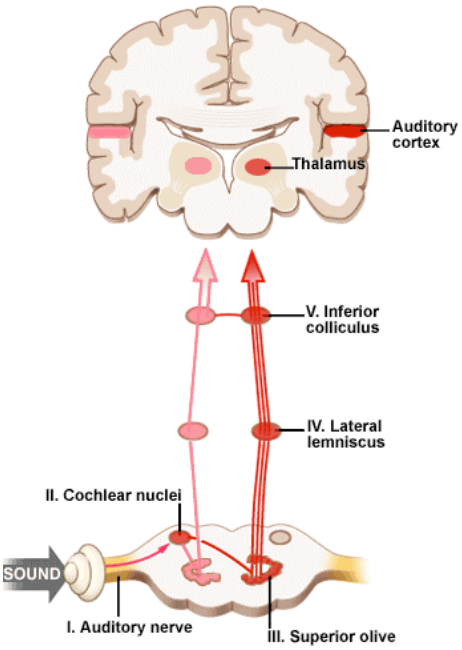


**Figure 1.** Auditory pathways from the cochlea to the auditory cortex. Patients who are deafened as a result of injury to the auditory nerve may be candidates for an auditory brainstem implant placed on the cochlear nucleus.[1]

### 1.2. Measurements of the responses of the auditory system

The response of the auditory system to stimulation can be analyzed using several different recording types, including far field or direct recordings. Auditory evoked responses are far field responses resulting from the postsynaptic currents occurring when large groups of neurons are simultaneously activated along the auditory pathway. The first 10 ms of the recordings obtained with two surface electrodes on the vertex and the ipsilateral ear of the subject are generated by the activation along the brainstem, up to the auditory cortex. These multi-peaked responses, called auditory brainstem responses (ABR), are widely used clinically to evaluate the integrity of the peripheral auditory pathway. During auditory brainstem implant (ABI) surgery, the ABR is the clinical measure used to determine if the central auditory pathway is being successfully stimulated.

Like in EEG recordings, many trials are averaged to eliminate the majority of the noise. In the normal human ABR, 5 main waves can be discriminated, followed by two smaller waves. The main waves are generated in specific locations in the auditory pathway, in the ipsilateral or contralateral side of stimulation, reflecting the temporal pattern of activation of the different auditory brainstem structures following stimulation. [4] The first waves are generated in the ipsilateral auditory nerve, while the following waves are the result of activation in higher structures. [4] The precise identification of the structures generating each wave is being investigated in animal models by lesion studies. [5]

In small animals, differences in the ABR occur compared to humans, due to anatomical differences in the auditory pathway. [4] In particular, the second discriminable peak on rats ABRs corresponds to the third wave in human ABRs, because of the small size of the head of these animals. This peak, labeled P2, is the largest peak in rats ABRs and can be used as a reference for the analysis. [6]

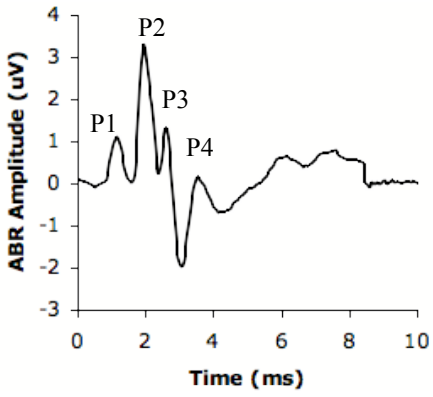


**Figure 2**. Example of normal rat ABR generated by acoustic click stimulus at 70dB, showing the labeled peaks.

In the human ABR analysis, the parameters used to characterize the signal are based on the three most visible waves, I, III and V. The latencies of these peaks and between them are especially used, as well as their amplitudes.[7] The threshold of activation is also an important measure.

The ABR requires strong synchronous activation of large groups of neurons, specifically the bushy cells of the cochlear nucleus (CN). It is then not suitable for the detection of small responses that may not necessarily strongly activate the whole auditory pathway. It is also not a good recording type at high pulse rate because the responses last for a relatively long time, leading to superposition of successive responses in the averaged signal. A technique activating other types of neurons than the bushy cells would not generate any ABRs, although the activation may be occurring.

Direct electrophysiological measures at a determined stage of the auditory processing have also been used in auditory research to provide precise information about the activation of the auditory pathway. The structure often chosen for these measurements is the central nucleus of the inferior colliculus (IC).[8] The accessible tonotopic axis of this auditory structure in the midbrain allows a frequency specification of the recorded responses, with a multichannel recording electrode inserted along the tonotopic gradient of the IC. This way, each channel records primarily the activation generated by a precise sound frequency. Moreover, the signals traveling along the different pathways of the auditory system all activate the IC, which makes it an 'obligatory' station for any activation traveling along the auditory system, even when ABRs are not generated.

This type of recording gives an insight into the frequency specificity and frequency encoding along the auditory pathway in the brainstem and midbrain. It has been used in several studies involving stimulation of the cochlea, either with infrared neural stimulation (INS) [8] or acoustic and electric stimulation [9]. The effect of hearing loss on IC receptive fields reorganization has also been investigated with this technique [10, 11], as well as the IC response following multichannel electric CN stimulation [12].

### 1.3. Replacement of Hearing in Deaf Individuals

Most sensorineural deafness in humans results from damage to the hair cells. However, a significant portion of deafness is caused by damage to the auditory nerve. Depending in the site and level of the damage, restoration of hearing will be achieved through different methods.

The most successful example of a bionic device to restore a special sensory organ in humans is the cochlear implant (CI). Patients who benefit from the CI are those infants, children and adults with severe to profound sensorineural hearing loss in both ears. The CI electrode is surgically placed into the scala tympani of the cochlea to directly stimulate the adjacent spiral ganglion cells, bypassing the nonfunctioning hair cells. Modern speech processing technology and the multichannel electrode placed along the basilar and middle turns of the fully-formed cochlea takes advantage of the tonotopic organization of the cochlea. Over 200,000 devices have been placed worldwide, providing meaningful sound and speech perception for adult and pediatric patients who would not benefit from conventional amplification. [13]

The auditory brainstem implant (ABI) is a type of auditory implant that can be used in patients who are not eligible for a CI. [14] Most commonly, patients with Neurofibromatosis Type 2 (NF2), a devastating autosomal dominant condition associated with the growth of benign bilateral vestibular schwannomas that compress the cochlear nerve, can beneficiate from ABI implantation. [15] In these patients, removal or growth of these tumors often destroys the auditory nerve, meaning that these patients are not able to use a hearing aid or CI. [16] The ABI bypasses the cochlea and auditory nerve and targets the surface of the CN. NF2 is the only condition for which the ABI is approved by the Food and Drug Administration (FDA) in the US. In other countries, some patients who suffer from other conditions than NF2 and whose hearing cannot be helped by conventional hearing aids or CIs could also beneficiate from ABI implantation. These conditions include cochlear aplasia, in which the cochlea is unimplantable, cochlear

nerve agenesis, which results in a damaged VIIIth nerve, or VIII nerve sectioning due to trauma. [17]

### 1.4. The ABI – current devices and challenges

Current ABI devices consist of an externally worn system that includes the microphone, speech processor and batteries, and a surgically implanted receiver-stimulator that delivers encoded information to the electrode array. This electrode array, with contacts made of platinium-iridium alloy, is placed during surgery on the surface of the CN by

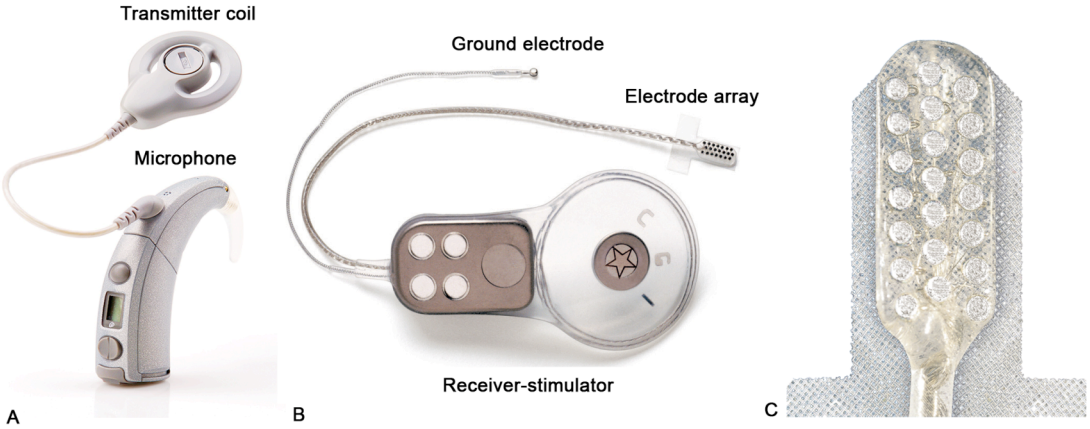


**Figure 3.** Auditory brainstem implant (ABI) system. A- speech processor (worn over the ear), B-surgically implanted receiver-stimulator, and C-magnified view of surface electrodes on a nonconformable silastic paddle, placed on the cochlear nucleus during surgery. *Modified images courtesy of Cochlear Corporation.*

access via the lateral recess of the fourth ventricle. When activated, the electrodes transmit electrical stimuli that depolarize neurons of the CN, resulting in sound awareness in the majority of ABI users. There is a tonotopic arrangement in the CN but due to its three-dimensional configuration accessing specific frequencies from the surface of the CN with ABI electrodes is more challenging than with the CI.

During ABI placement surgery, auditory evoked potentials are intra-operatively monitored to guide the correct positioning placement of the electrode paddle. The goal is to have as many electrodes as possible placed on the surface of the CN and generating electrically evoked multi-peaked ABRs. After implantation, when the implant is switched on, non-auditory sensations can appear because of current spread that activates nearby cerebellar structures or cranial nerves, and are often associated with longer latency broad-peaked responses to intra-operative monitoring. To avoid these side effects, only the electrodes giving good auditory sensations without non-auditory side effects are selected and activated. [18]

In most patients, useful hearing sensations are obtained with an ABI. These sensations can be used for environmental sound awareness as well as temporal cues and as a support to lipreading. [19] In a few patients, the implant even allows a good speech understanding without lipreading. [14] One idea is that the ABI is limited by the spread of the current, leading to non-auditory side effects and smeared hearing perception due to the activation of large neuronal populations. One way to improve this would be to decrease the threshold of current necessary for activation. For this purpose, penetrating ABIs have

been developed and tested. The hypothesis was that it would also give a better access to the tonotopy of the CN, thus hopefully improving performance. Results showed that the current thresholds for stimulation were indeed lower with the penetrating ABIs. However, no improvement in speech understanding was found, so this strategy was abandoned. [20] Continued work on surface ABIs thus needs to be done to improve performance.

### 1.5. INS mechanism and early work

The use of several optical stimulation methods has been investigated in an attempt to achieve a better spatial resolution in neuronal stimulation. One of these methods is the infrared neural stimulation (INS). This technique was first demonstrated in 2005 by Wells et al, who used pulsed low-energy infrared laser light to stimulate a rat sciatic nerve. [21] The main advantages of this technique are the spatial selectivity of the stimulation, the absence of electrical stimulation artifact and the absence of contact of the optical fiber and the tissue during stimulation. [22]

The mechanism by which infrared laser light activates neural tissue is the focus of current research. Recently described by Shapiro et al, [23] is a general electrostatic mechanism. This theory is based on the fact that the water in the tissue absorbs the energy deposited by the laser, inducing a local increase in the temperature.[24] This effect transiently increases the membrane capacitance, inducing depolarizing currents. It is then an intrinsic property of the membrane and the initial depolarization of the neurons does not fundamentally require membrane channels. To generate action potentials, however, neuron membrane channels are obviously necessary.

INS has been investigated for several applications in the peripheral nervous system, including embryonic heart pacing [25], facial nerve stimulation [26], vestibular hair cells stimulation [27] and cavernous nerves stimulation [28]. To increase the range of possible intensities to activate nerves without reaching the damage threshold, the use of combined sub-threshold electrical stimulation and infrared pulses has been investigated. This method decreases the optical activation threshold while maintaining the high spatial precision achieved with INS alone. [29]

INS has also been investigated as a means to stimulate the central nervous system in vivo. A study using INS on the somatosensory cortex of anesthetized rats showed a significant inhibitory effect in the neurons firing rate. This effect could be expected, since the laser at the wavelength used deposited energy in inhibitory layers of the cortex. [30] At low laser powers and low pulse rates, INS has been shown not to induce damage to the tissue. [31] It is then a safe method of nerve stimulation, with promising clinical and research applications.

### 1.6. INS and peripheral auditory system

The use of INS has been investigated in the peripheral auditory system by the pioneering work of Claus-Peter Richter, who uses this technique to stimulate spiral ganglion cells in the cochlea. A parametric study was performed to determine the effect of changing pulse width, pulse rate and laser wavelength on the activation. [32, 33] The same group also found an increased selectivity of INS over electrical stimulation by cFOS staining in

spiral ganglion cells. [34] Finally, increased spatial selectivity of INS was shown by IC measurements following intracochlear INS. [8] A possible application of this technique would be to optically stimulate the spiral ganglion cells in the cochlea, in an effort to develop a new-generation cochlear implant. [35]

Recently, an acoustic artifact intrinsic to the pulse generation in INS has been described. This effect can be as high as 60-70 dB SPL in air and is due to the rapid heating of the air at the tip of the fiber during the energy change that forms the pulse, in thermal confinement conditions. [36] This effect, known as optophonia, has to be taken into account, especially in the experiments involving the auditory system. The effects of acute and chronic deafening during stimulation of the peripheral auditory system have been studied, in order to identify the precise acoustically generated component of the responses. [37]

### 1.7. General aims of the project

The first aim of this project is to use INS on the surface of a rodent CN to see if its auditory system can be activated by this means. Both far-field responses and direct electrophysiological measures in the IC are used to characterize the responses to INS with different parameters and at different stimulation locations. Because of the potential acoustic artifact associated with INS, known as optophonia, we will also perform studies in acutely deafened subjects.

## 2. Materials and methods

### 2.1. Model of the cochlear nucleus

A 3D model of the cochlear nucleus is constructed using the AMIRA software (AMIRA, Mercury Computer Systems, Berlin, Germany, Version 5.4.2). For this purpose, 40μm thick slices of the right brainstem of a sprague dawley rat are used. First, pictures of the slides are taken under a microscope with a magnification of 1.5 and loaded into the software. Successive images are then aligned manually and the segmentation is performed in order to delimitate and identify the different subdivisions of the CN complex (Dorsal CN, Antero-ventral CN, Postero-ventral CN and auditory and vestibular nerve entrances into the CN). The subdivisions were identified according to the criteria defined by Hackney, et al. [38] for the guinea pig, and a rat brain atlas.

A surface model is then generated and smoothed with software functions. Images in a 3D representation and in 2D planar representations from different perspectives are taken. Measurements are made for the volume of each part and the dimension of the different subdivisions and the CN in general

### 2.2. Anesthesia and surgery

Surgeries are performed by my colleague Dr Rohit Verma, postdoctoral research fellow at MEEI, on Sprague Dawley rats. Anesthesia is administered using an intraperitoneal injection of Ketamine and Xylazine and further booster doses are administered

intramuscularly based on paw pinch responses. Acoustic ABR is first obtained and then the tracheotomy is performed. The CN is then exposed by performing an occipital craniotomy and suctioning part of the cerebellum to reveal the surface of the CN.

The IC is accessed using a stereotactic approach. A square craniectomy of approximately 5mm x 5mm is created using a craft drill on the contra-lateral side to the exposed CN. The craniectomy is situated on the right arm of the Lambda suture such that the suture forms the posterior third of the craniectomy. The saggital suture is approximately 1 mm from the medial border of the craniectomy. (Figure 4)

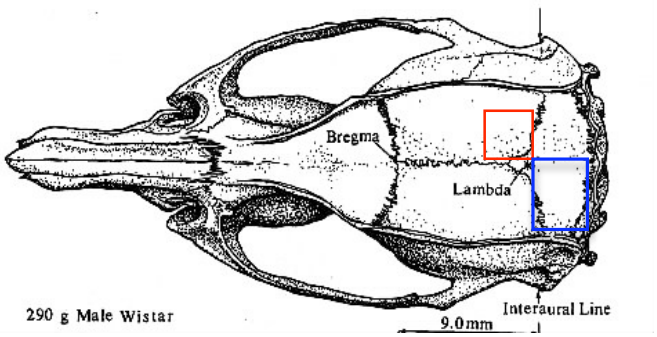


**Figure 4**. Rat cranium showing the approximate positions of the craniectomies performed to access the CN (blue) and the IC (red).

The manipulating arm of the stereotactic headholder is oriented such that the electrode enters the cerebrum in a dorso-ventral direction in order to access the tonotopic organization of the central nucleus of the inferior colliculus (ICCN). The electrode is slowly advanced into the ICCN and its correct placement is confirmed before each experiment to make sure that the electrode was placed along the tonotopic axis of the ICCN. If the electrode array is correctly placed along this gradient, a shift of the activation profile is visible as the frequency of stimulation is changed.

## 2.3. Stimulation

### 2.3.1. Technical specifications for INS and Electrical

Infrared pulses are generated using a diode laser (Capella R-1850, Lockheed-Martin Aculight Corp., Bothell, WA). The left CN is stimulated by surface contact with the tip of the optical 400μm fiber. In all cases, the order of the runs is pseudo-random.

Electrical stimuli were 50-μs anodic current pulses generated by passing the output of a 16-bit D/A converter (PXI-6221, National Instruments, Austin TX) through an analog stimulus isolator (Model 2200, A-M Systems, Carlsborg WA). Current pulses were delivered to the exposed CN using a parylene-insulated platinum-iridium twisted electrode (51mm length, impedance = 0.1-0.5 MΩ) (Microprobe Inc., Gaithersburg, MD). Bipolar stimuli were presented at 5 pulses per second, and varied in amplitude from 0 to 0.4 mA.

### 2.3.2. Parametric studies

Studying the effect of the different stimulation parameters can give valuable information regarding the properties and mechanisms of this stimulation. The effect of varying the pulse width, laser peak power, laser wavelength and pulse rate are then studied.

*Radiant energy series*

Knowing that the radiant energy per pulse brought to the tissue is determined by a combination of three parameters, laser peak power, wavelength and pulse width, the first interest of this parametric study is to vary each of these parameters independently to determine the dependence of the response to each of them. The main question is to know if the response is dependent only on the total radiant energy, which means varying any parameter would have the same effect, or if the variations of those parameters have different effects on the response. This is possible mainly with the laser peak power and the pulse width, the range of wavelength available with our laser being very limited (1849 to 1865nm). The range of energies reached by varying the wavelength is therefore very small. In this section, only the effect of the laser peak power and pulse width will then be compared, with radiant energies varying from 0 to 711mJ/cm$^2$ by varying the pulse width from 0.05 to 0.4ms and the peak power from 0 to 70% (0 to 2844 mW/cm$^2$)

*Wavelength series*

This parameter will be studied by varying it in two different ways. First, the total energy brought to the tissue will be kept constant by adapting the laser peak power. Second, only the wavelength will be varied, leading to a change in total energy. Although the range of wavelengths is very limited (1849nm to 1865nm) and the range of energies will be small too, a possible effect could be found due to the difference in absorbance of the tissue at different wavelengths. The variation in absorbance leads to penetration depths varying from approximately 1100 to 600 μm.[39]

*Low pulse rate series*

We are also performing pulse rate series, at pulse rates from 3 to 63 Hz, to determine if increasing the pulse rate, which will increase the total energy brought to the tissue, has an influence on the response. The pulse widths for stimulation have been carefully chosen to prevent a 60Hz noise contamination, by avoiding multiples of 60.

*High pulse rate series*

A specificity of IC parametric studies is the possibility to record the response to burst of pulses at high pulse rate – up to 500Hz, to approach the physiological range. This is not possible to record with ABRs due to the far field nature of this type of recordings. The question asked is on what parameters does the response mostly depend in this case. To answer that question, the total energy brought to the tissue at different pulse rates will either freely vary, or will be kept constant by compensating the change in total energy with pulse width or laser peak power changes.

*Specifications for ABR studies*

A set of reference parameters is defined based on previous work, and will be used to normalize the data and as a quality control. During all the ABR experiments, reference responses are recorded regularly – every 6 to 7 runs. These references are always done with the same parameters, known to give high amplitude ABRs, and have two main uses. The first is to ensure a constant data quality during the experiment, to make sure the laser fiber hasn't moved, especially after the rat was given an anesthesia booster dose. The second is to allow a normalization of the parameters, in order to have comparable data from rat to rat. This will be further explained in the "analysis" part of this report. These parameters are also the default parameters, whenever they are not specifically mentioned.

### 2.3.3. Location studies

Another goal of these experiments is to determine whether the response is dependent on the stimulation site on the surface of the CN, with electrical stimulation as well as INS. The CN surface is roughly 1x2mm. To have reliable and repeatable stimulation sites, a virtual grid is defined, which contains 3 rows and 4 columns (see figure 5). The reference point for this grid is the posterior end of the 4th ventricle, close to the site C4. This site is always fully exposed during surgery. The site A1, the most rostral and lateral, is called the "sweet spot". It corresponds to the nerve root in the CN. The ABR parametric studies are performed at this spot, because it was shown in previous work to give reliably high ABR amplitudes.

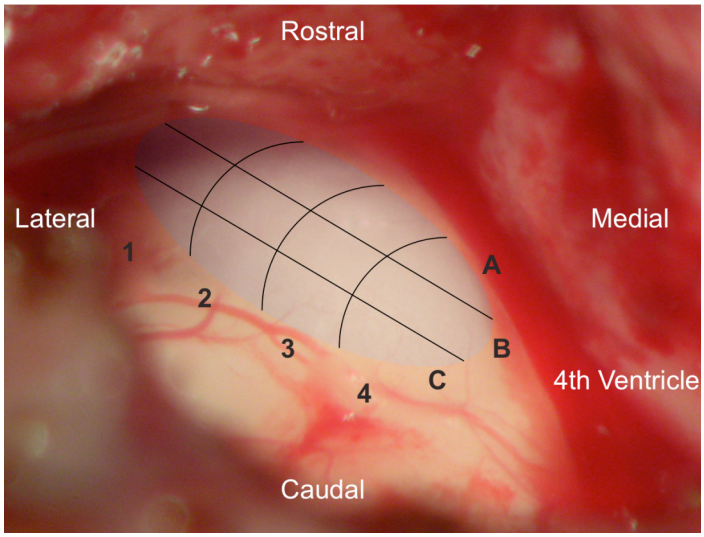


**Figure 5**. Virtual grid used on the CN to have reliable stimulation sites for the location studies

At each stimulation site on the CN, data are recorded with both IC and ABR techniques, in order to have all the possible information from this site. The ABR and IC runs performed during the parametric and location experiments are shown in Appendix 1 and 2.

### 2.3.3. Optophonic artifact measurement

To characterize the acoustic artifact occurring during the laser pulse generation, measurements in air were made with a microphone placed 1mm away from the tip of the fiber, in a perpendicular configuration. This configuration, in which the laser beam is not directed towards the microphone, is used to avoid any kind of artifact of the laser beam on the microphone. This noise is characterized at the reference parameters, and for a laser peak power series from 0 to 70%, a pulse width series from 0.05ms to 0.4ms and a wavelength series from 1849nm to 1865nm to match the data obtained in the parametric studies.

### 2.3.4. Deafening

Since an optophonic artifact is occurring during INS pulse generation, the same parametric and location data have to be obtained in deafened rats, to eliminate a possible acoustically generated component to the response. The rats are mechanically deafened by dividing the cochlear nerve as it exits the internal auditory meatus. To ensure that the acoustic pathway is intact from the CN onwards, the similarity between electrically generated ABRs obtained at the same site in the pre- and post-deafened animals is checked.

## 2.4. Signal recording specifications

### 2.4.1. ABR

Three needle electrodes are used to record the ABR. One is placed on the vertex of the subject's skull, the second one is placed behind the ipsilateral ear and the third one, the ground, on the back of the animal. The ABR signal is measured between the two first electrodes, relatively to the reference electrode.
The signal is amplified with a 40 dB gain and analog filtered with cutoff frequencies of 30Hz – 3kHz (Ithaco Model 1201, DL Instruments, Ithaca NY) before being converted to digital with 16-bits resolution at 25 kHz (PXI-6221, National Instruments, Austin TX).

### 2.4.2. IC

The recordings from the contralateral IC are performed with a silicon-substrate thin-film 16-channels penetrating electrode (A1x16-5mm-100-177, NeuroNexus Technologies, Ann Arbor, MI) inserted along the tonotopic axis of this structure. Each recording site has a surface of 177$\mu m^2$ and the center-to-center interval is 100μm. A global reference is used, which is the average of all the signals. They are then converted to digital with 16-bits resolution at 20 kHz, and the raw data are stored in the system.
Once the electrode is inserted in the IC, it has to be acoustically tuned in order to confirm the placement and to know the characteristic frequencies corresponding to each channel. This is done with pure tones at specific frequencies to the left ear. The range of frequencies used is 1 to 32 kHz, with 2 frequencies per octave.

## 2.5. Signal processing and data analysis

### 2.5.1. ABR

*Initial processing*
Data analysis is performed with programs written with the Matlab software (Mathworks, Natick, MA). The ABR signal analysis is critical to detect the waveforms and to extract meaningful parameters from the signal. The goal is to remove the noise (mainly electrical, EEG and EMG noise) as much as possible in order to increase the Signal-to-Noise Ratio (SNR). The first step to remove the noise is averaging, a technique widely used in evoked potential analysis. [18] The assumption is that the signal does not change among trials, so it will add up whereas the noise is stimulus-independent, so it will be cancelled out by the averaging. 500 sweeps are averaged for each run, which has been shown in previous work to be sufficient to remove most of the noise [32]. To further enhance the SNR, filtering can be used. During data acquisition, analog filtering has to be used over a very broad bandwidth to avoid waveform distortion (30Hz to 30kHz). [40] Digital, phase-invariant filters are preferred because they avoid phase distortion. The cutoff frequencies have to be optimized in order to maximize the SNR and minimize the signal amplitude distortion.

For this purpose, a useful technique is to analyze the signal frequency spectrum after application of the Fast Fourier Tansform (FFT) on the signal, to detect the frequencies contributing to the actual signal and those contributing mainly to the noise.

The filtering is done with a forward and reverse Butterworth filter of order 5. The cutoff frequencies have been determined with the FFT (Fast Fourier Transform) spectrum, in which the frequencies containing most of the signal were selected, over many trials. Different cutoff frequencies are used for optically and electrically generated ABRs, due to the different properties of the signal. For the INS generated ABRs, the cutoff frequencies maximizing the SNR and minimizing the signal distortion are 100Hz and 1.4kHz. For the electrically generated ABRs, the cutoff frequencies are 200Hz and 2.5kHz. Additionally, in the electrically generated signals, the first millisecond of recording after stimulation onset is removed before filtering, as it mainly contains the stimulation artifact and would induce a waveform distortion in the signal if kept during filtering. This step is not necessary with optically generated ABRs, due to the absence of stimulation artifact. To take into account the different filtering parameters used in INS or electrically generated ABRs, the waveforms of these two types of signals will not be directly compared.

*Peak detection and review algorithm*

From the filtered ABR time-domain signal, several meaningful parameters can be extracted. For this purpose, the different peaks have to be detected. The detection technique used involves finding the points where the derivative of the signal is zero. These correspond to local maxima and minima of the signal. The different peaks can then be extracted and identified. There is one major peak very reliably present in the rat ABR generated with CN laser stimulation. This peak corresponds to the signal maximum, and was detected and labeled "P2" in the literature.[6] This terminology is also used here, so the highest amplitude peak is labeled P2. P4 is also specifically labeled, being the next big wave after P2. P3 is a small wave, not present in all the signals because it is often merged with wave 2 or 4.

The automatic detection and labeling of the peaks is manually reviewed to avoid detection errors, to ensure correct labeling of the waves, particularly when P3 is not present, and to identify signals with no response. The developed algorithm includes the possibility to add missing peaks, to change the P2 label and the other labels accordingly and to define the runs as "no signal", which sets the amplitudes to zero and removes the latencies from the analysis. Visually, the possible detection of P2 was considered as a response.

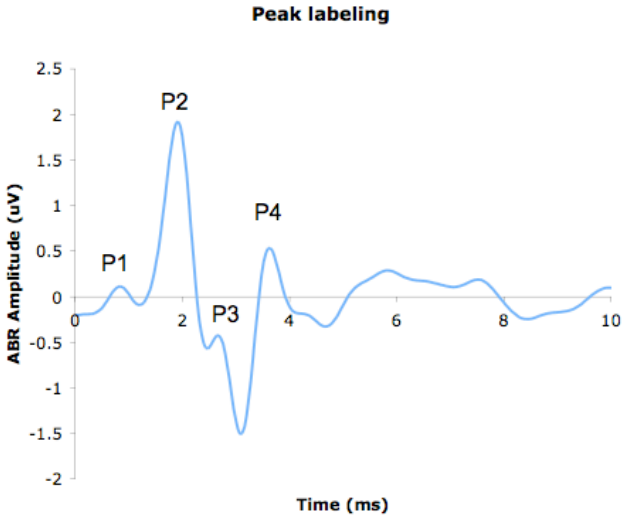


**Figure 6**. Example of peak labeling on an INS generated signal, at reference parameters (pulse width = 0.25ms, pulse rate=23Hz, wavelength=1849nm, radiant energy=711mJ/cm$^2$)

At this stage, a quality control on the data is performed. Using the runs with reference parameters performed every 7 run, the reliability of the P2 latency is assessed. Whenever this latency varies of more than 5% from the previous reference runs, the following data are discarded. Indeed, the latencies of the first waves has been shown to be extremely reliable under normal conditions, [4] and an abnormal variability would indicate a bad

data quality, which could have several possible origins, including a damaged cochlear nucleus, a damaged auditory pathway or a problem with anesthesia.

*Parameters extraction, normalization*

Once the different waves have been detected, several features can be identified from the signal to aid analysis. Two types of parameters are extracted, corresponding either to the waveform of the signal – wave amplitudes and latencies – or to the energy of the signal – RMS and percentage of energy in each wave [41]. The amplitude of a wave is defined, in keeping with standard practice, as the maximum of the amplitudes calculated with the previous and the following minima. The latencies are defined as the time between the stimulus onset and the peak of the wave. The RMS value of the signal is a measure of the mean signal energy and is calculated by taking the square root of the average value of the squared signal. The signal energy is calculated by the sum of the squared values in the interval. Once these parameters are extracted, a sub-group of parameters are selected for the subsequent analysis based on their reliability and their physiological significance. For example, P2 and P4 are reliably present in the signals, whereas P3 is not. Because of this, the latency and amplitude of P2 and P4 will be more relevant to analyze than those of P3. The list of analyzed parameters is then the following: amplitude and latency of P2 and P4, total amplitude of the signal, RMS energy of the signal, RMS energy of wave 2 and percentage of energy contained in wave 2. Wave 2 is defined as the signal present in the time between the local minima directly before and after P2.

One issue that has to be overcome when analyzing the parameters is the variability between subjects, which would strongly influence the data and hence has to be removed. This is achieved through normalization, which ensures that the data are comparable from rat to rat and from site to site. The normalization references are the parameters obtained every 7 runs with the reference stimulation parameters – pulse rate of 23 Hz, wavelength of 1849 nm, pulse width of 0.25 ms and laser peak power of 70%, which correspond to a radiant energy of 711 mJ/cm$^2$. Two different normalization values are extracted from the reference parameters runs: the amplitude and latency of P2. These are used for the normalization of respectively the amplitudes and latencies extracted from the previous and following signals. The signal energy values are not normalized.

### 2.5.2. IC

*Initial processing*

The recorded signal from the IC is composed of three major signal types. First, the activity from the neurons directly adjacent to the electrodes can be recorded in the form of spikes. The evoked potentials are also recorded by the electrodes, reflecting the post-synaptic potentials due to the synchronous activation of large groups of neurons along the auditory pathways. The evoked potential frequency is lower, so it can be removed by high-pass filtering with a forward and reverse Butterworth filter of order 5, with a cutoff frequency of 500 Hz. (figure 7)

Background noise from other sources is also present in the recorded signal. Its frequency is similar to the frequency of the spikes, so it cannot be removed by digital filtering. However, its amplitude is smaller than the spikes, so a proper spike detection method can minimize its influence on the data.

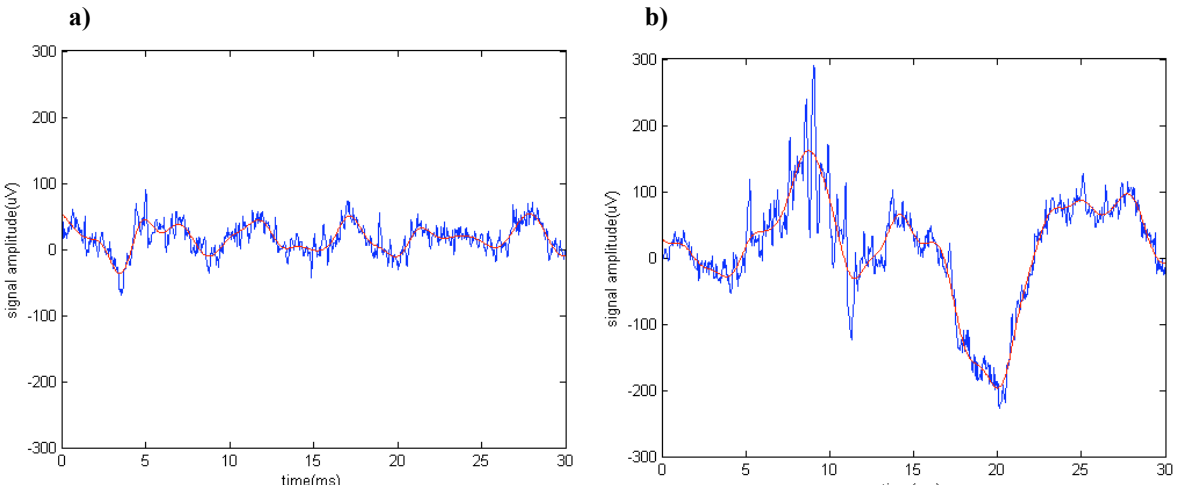


**Figure 7**. Examples of **a)** a signal with no significant activation and **b)** a signal with activation. In each plot, the raw signal is shown in blue and the low frequency component in red. The low frequency component, which mainly corresponds to the evoked potential, is filtered out.

*Spike detection threshold determination*

The general principle of the developed spike detection algorithm is to fix a threshold and count the number of times the signal passes this threshold [42] [8]. The threshold should be fixed high enough to be higher than the basal electrical activity recorded (without spikes), and low enough to be able to detect the spikes. A method based on the median of the absolute value of the signal is used, as it gives a reliable measure of the background noise without being too much affected by random spikes appearing even without activation.

For INS generated signals, the window chosen to calculate the threshold is the first 4 ms of the runs, as it was noticed that the activation only starts after about 5 ms. In the case of electrically generated signals, this window cannot be used because it mainly contains the stimulation artifact. A 4 ms window at the end of the recording is then used. For a given run, the threshold used was calculated with the average of the medians on this interval for the 32 trials. The median on the first 4ms interval was multiplied by a factor of 4 to set the threshold. This factor was selected as the one giving the threshold with the most reliable spike detection, being low enough to detect the spikes and high enough to ignore the noise.

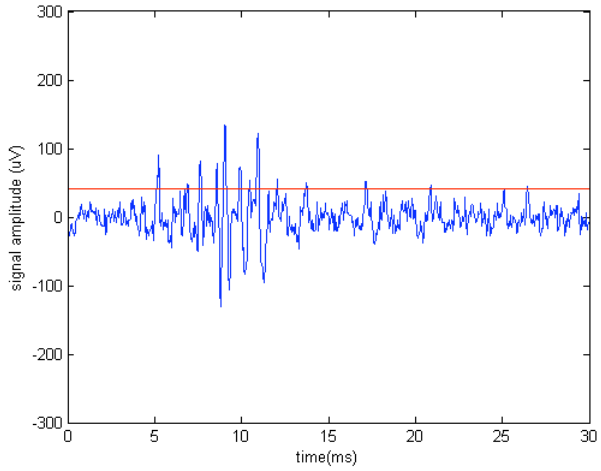


**Figure 8**. High-pass filtered signals (in blue) with threshold (in red) for a signal showing activation.

*Determination of the analysis time window*

To find the window in which the activation occurs, the PSTH (peri-stimulus time histogram) is used [12, 42]. The PSTH calculates the average number of spikes per time interval, over the different trials. The time interval was fixed to 1ms. Figure 10 is an example from the data showing the PSTHs in a color plot for the different stimulation frequencies and the 16 recording electrodes. Following analysis of several datasets using the PSTHs, a window of 5 to 25ms is chosen for the analysis. The activation at each level, frequency and electrode is then defined as the average of the spike counts over this 20ms window.

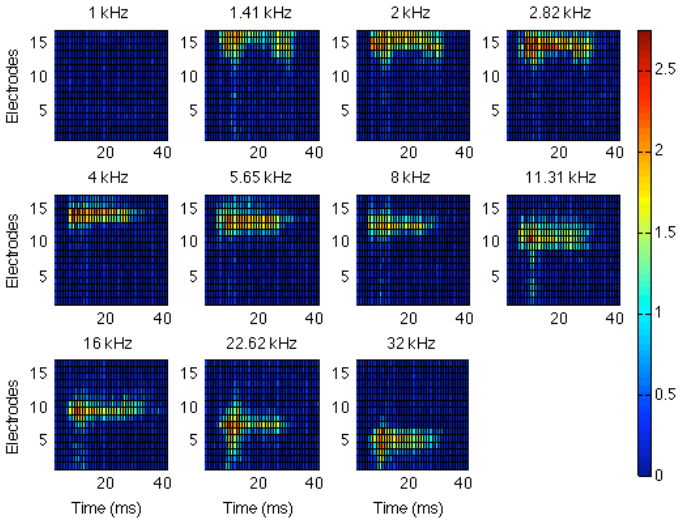


**Figure 9**. Example of IC activation recorded following a 70dB stimulation at frequencies varying from 1 to 32 kHz. The main activation seems to occur between 5 and 25ms after stimulation onset.

This window is not used for the analysis of high pulse rate series, as the stimulation is repeated during 100ms for each run. Instead, the average activation is calculated for each millisecond of the run. The time dependence of the average activation following high pulse rate stimulation can then be plotted and analyzed. In particular, the average spike count when the activation reaches a plateau at each wavelength will be compared between the different conditions – varying pulse width, laser power or total radiant energy to assess the effect of each of these parameters at high pulse rate.

*Post-processing*

In order to extract reliable parameters from the IC data obtained, several post-processing steps are used. First, the spontaneous activity is defined as the average of the spike counts at the zero stimulation level across the electrodes. The standard deviation of the baseline activity is also calculated, before subtracting the spontaneous activity to all the values. A threshold is then defined, and all the values below this threshold are set to zero. This threshold represents the significant activation level and can be defined either with a multiple of the standard deviation of the spontaneous activity [42], or by a percentage of the spontaneous activity [10]. In this analysis, the threshold was fixed to four times the standard deviation of the baseline. Since there is no objective way to determine the exact value of the multiplication factor of the standard deviation, it is determined by testing several different values on several datasets and choosing the value that provides the best discrimination between noise and signal. The important point here is that the same factor is used uniformly in every dataset, to guarantee that the data are comparable.

*Parameters extraction*

Several parameters are then extracted from these profiles. First, the activation threshold is defined as the lowest level of a peak power series triggering a significant activation in at least one electrode [42]. The characteristic frequency is then defined as the frequency corresponding to the electrode with the highest activation two steps above the threshold

[11]. These two steps correspond to 10dB in the acoustic experiments and to 10% of the laser peak power in the INS experiments [42]. The width of activation at this level, which is calculated with the number of activated electrodes, is also obtained [8]. The fourth parameter extracted is the mean spike count across the 16 channels for each stimulation level, which gives an indication of the averaged activation in the IC in a frequency-independent way. This last parameter is obtained before applying the thresholding step in the post-processing algorithm. The baseline level is then removed, but the non-significant values are not set to zero.

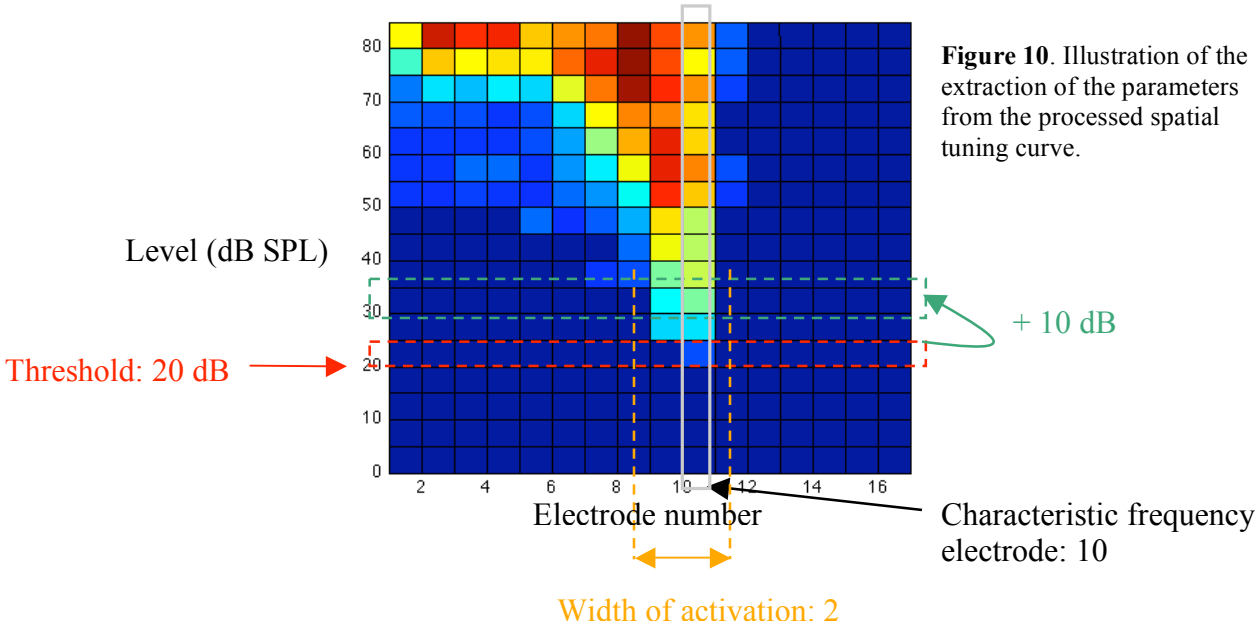


**Figure 10**. Illustration of the extraction of the parameters from the processed spatial tuning curve.

### 2.5.3. Statistical analysis

The statistical test used to analyze the data is a one-way or n-way analysis of variance (ANOVA) test, as used in other referenced work. In the case of comparison of means between more than two groups, a Tukey's honest significance test is then used to assess which means are statistically different from one another.

## 3. Results

### 3.1. Model of the cochlear nucleus

A 3-dimensional model is created to identify the visible structures during the surgical approach of the CN. The geometry of the anatomical subdivisions as well as their relative positions are important to determine which structure could be the target of INS or electrical stimulation during the experiments.

Measurements of the size of the different subunits of the CN are performed, as well as estimations of the volume of each subunit. Figure 10 shows a 3-dimensional representation of the CN with the auditory and vestibular nerve entrances. The different anatomical subdivisions are represented in different colors. Figure 11 demonstrates the surgical view available during the experiments. The surface most readily accessible for

stimulation is the dorsal cochlear nucleus (DCN). An estimation of the volume of each part, as well as measurements from 2-dimensional views of each part of the CN can be seen in appendix 3.

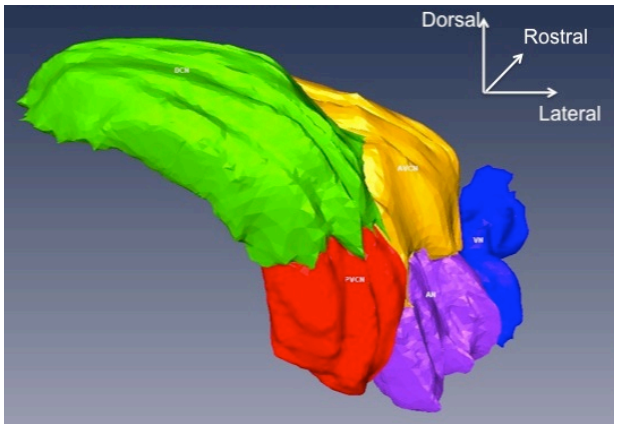


**Figure 10.** 3-dimensional representation of the CN showing the DCN in green, the PVCN in red, the AVCN in orange, the auditory nerve entrance in purple and the vestibular nerve entrance into the brainstem in blue.

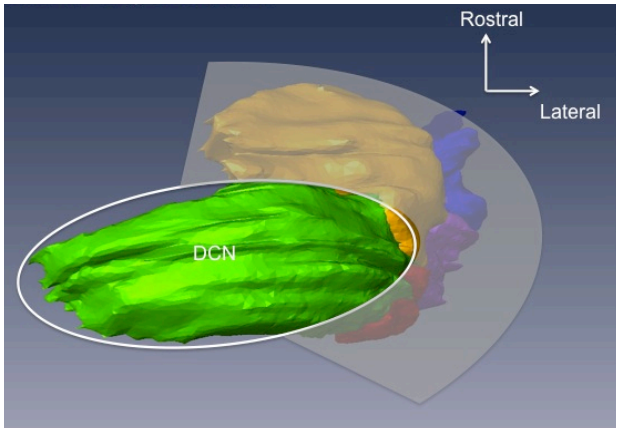


**Figure 11.** Surgical view of the CN obtained during the experiments after the posterior craniotomy and cerebellar aspiration. As seen on this 3-dimensional model, the accessible part of the CN (non-shaded area) is mainly the DCN.

Figure 11 shows a representation of the surgical view achieved during surgery, in which the main exposed part is the DCN. All the results obtained with CN stimulation presented in this report are actually obtained with DCN stimulation. However, the terminology used will still be 'CN stimulation'.

### 3.2. ABR tests of hearing sensitivity

At the beginning of each experiment, an acoustic ABR is obtained in the subjects to assess the integrity of the auditory system. Only the animals with a threshold lower than 40dB SPL were used. The 31 animals used for this study had a threshold between 25 and 40dB SPL, with an average of 30.4±0.87dB SPL. Figure 12 shows an example of acoustically generated ABR.

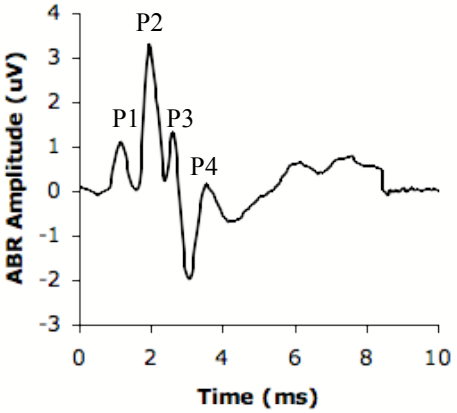


**Figure 12.** Example of acoustically generated ABR at 70dB, with a click stimulus presented during 20ms.

### 3.3. IC responses to acoustic stimulation

Profiles of IC activation after stimulation at different acoustic frequencies were obtained at the beginning of each experiment. In response to high frequency sound, IC activation occurs maximally in the deepest electrodes (low electrode numbers), and for lower frequencies, activation is seen in more superficial electrodes (higher electrode numbers). An example of spatial tuning curve obtained is shown on figure 13a, with the correspondence between electrode number and depth in the IC shown on figure 13b. To highlight the shift of activation profile, figure 14 shows the activation obtained at a stimulation level of 50dB SPL, for each frequency.

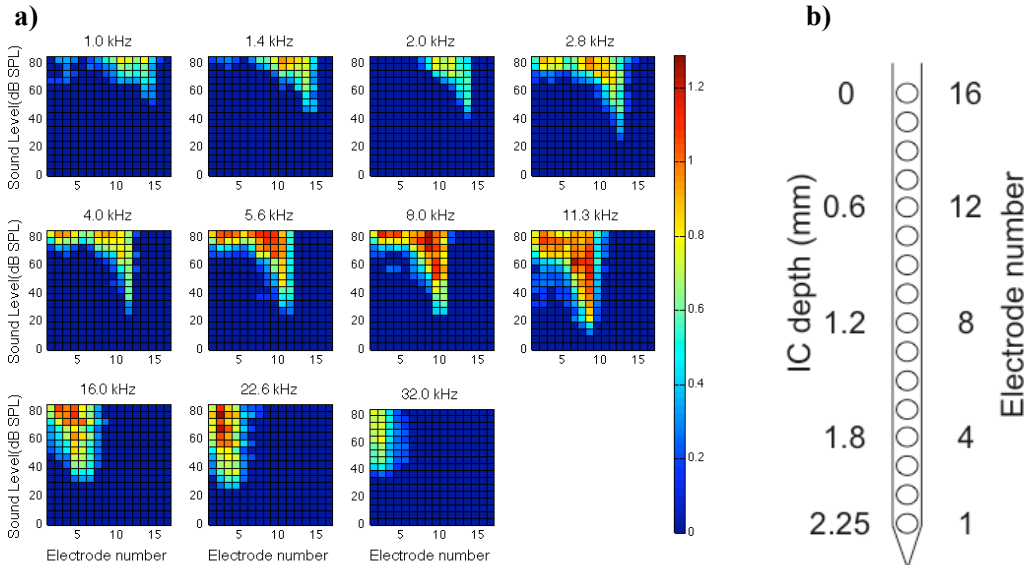


**Figure 13**. **a)** Example of two-dimensional mapping representing, for each acoustic frequency, the average spike count for each electrode and stimulation level. The color scale shows the lowest average processed spike counts in dark blue and the highest in dark red. **b)** Schematic representation of the 16-channels electrode, showing the correspondance between the electrode number and the depth in the IC.

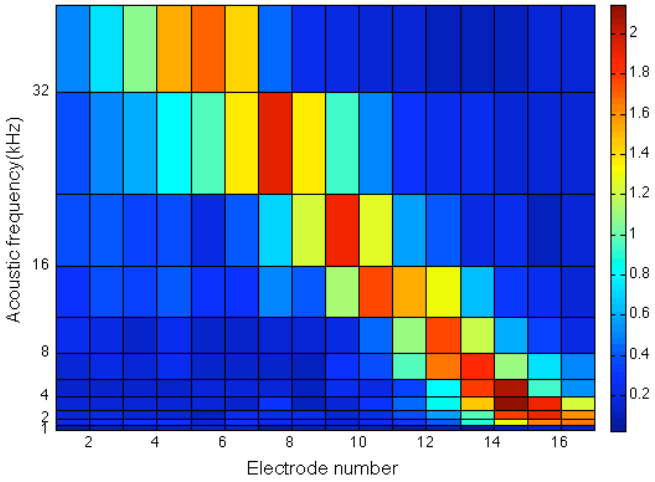


**Figure 14**. Average spike count calculated for the 16 electrodes and the different acoustic frequencies of stimulation (1 to 32 kHz), at a stimulation level of 50dB SPL. The shift of activation is clearly visible, with high frequencies activating maximally deep electrodes (low number), and low frequencies activating maximally shallow electrodes (high number).

This type of activation shift was tested in every experiment, and preparations showing lack of a shift were not used. Correct placement of the electrode is essential to ensure high quality data acquisition. Figure 15 shows for all experiments that were used, the

characteristic electrode extracted for each acoustic frequency. In each case the tonotopic activation is clearly visible, which confirms that the electrode array is correctly placed.

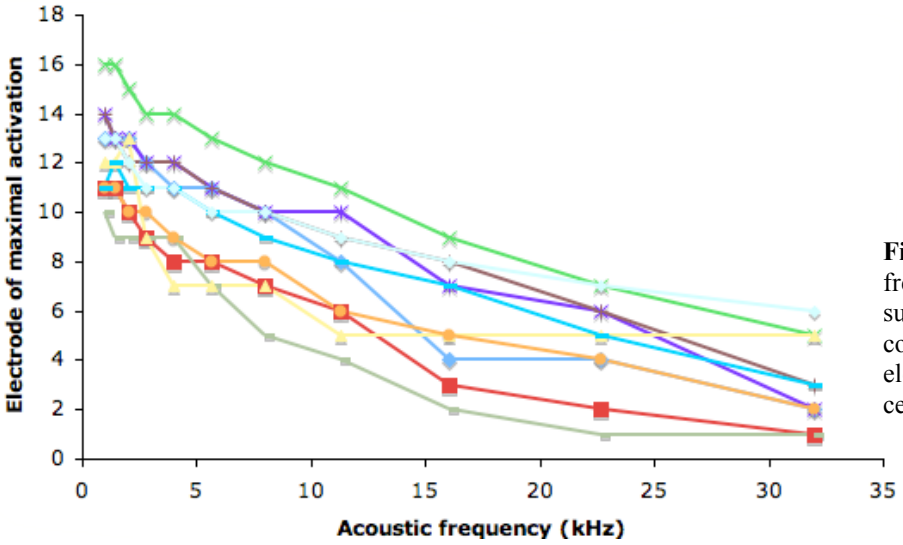


**Figure 15**. Electrode-frequency mapping for 9 subjects confirming the correct placement of the 16-electrodes array into the central nucleus of the IC.

## 3.4. ABR Responses to INS

### 3.4.1. General

When the CN is stimulated with the INS, ABRs can be recorded. Multiple peaks can be identified and labeled from the signals (see figure 16). These peaks have big similarities with the peaks identified from the acoustically generated ABRs, and can then be labeled the same way.

### 3.4.2. Parametric studies

*Radiant energy series*

The first parametric series is a radiant energy series, performed by varying either the laser peak power or the pulse width. Figure 16 shows an example of superimposed traces from a peak power series and a pulse width series, with the P2 and P4 labelings. In this example, the ABRs at different laser peak powers appear very different, whereas the pulse width change does not appear to have an effect on the main peaks of the ABR waveform.

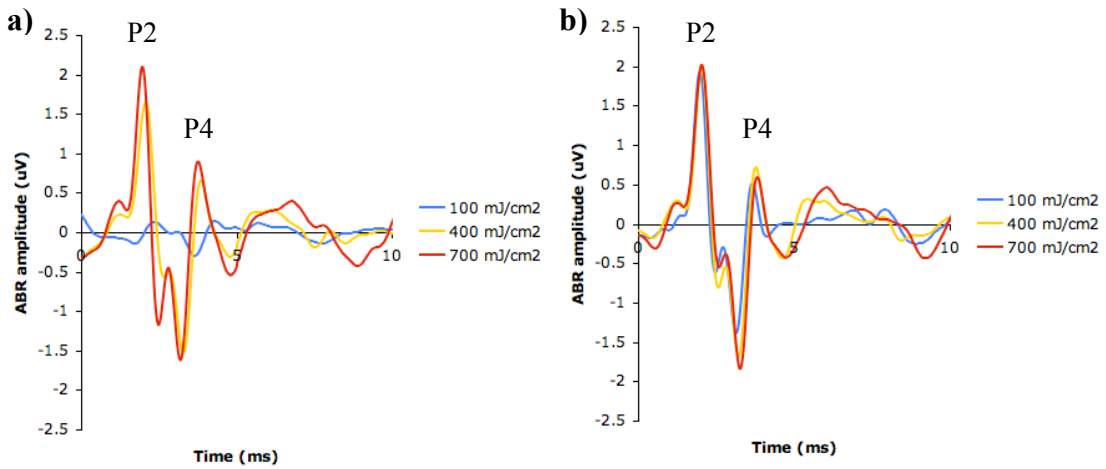


**Figure 16**. Example of ABR responses to **a)** a laser peak power series and **b)** a pulse width series. The laser peak power is varied from 0 to 70%, and the pulse width from 0.05ms to 0.4ms. All the non-varying parameters are kept constant at the reference values, i.e. wavelength: 1849nm, pulse width: 0.25ms, laser peak power: 70%, pulse rate: 23Hz. This corresponds to radiant energies between 100 and 700 mJ/cm$^2$.

The effects of these parameters on the P2 and P4 amplitudes and latencies are shown on figures 17 and 18. P2 and P4 are the peaks that are the most reliably extracted from the signals. As the laser peak power is increased (figure 17), the amplitude of P2 increases significantly. An increase in the amplitude of P4 can also be seen on the chart, but it is not statistically significant ($p>0.05$, see figure 19). This significant effect on the amplitude of P2 is not found in the pulse width series data, in which a change in pulse width does not have any significant effect on the amplitude of P2 and P4.

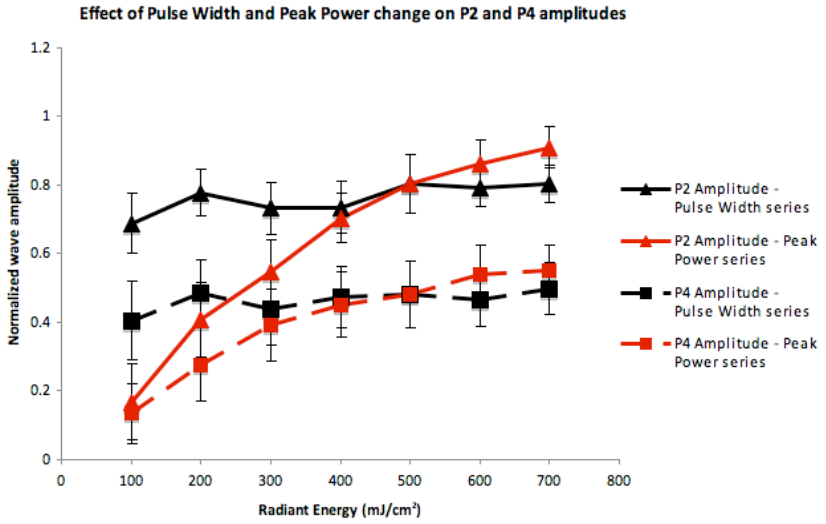


**Figure 17**. Effect of laser peak power series (red) and pulse width series (black) on the amplitude of P2 (full lines) and P4 (dotted lines). N=8 datasets

As the laser peak power increases, the latency of P2 significantly decreases ($p<0.05$, see figure 19). The same tendency is found for the latency of P4. However, it is not statistically significant ($p>0.05$). The pulse width series does not show a significant effect on the latencies.

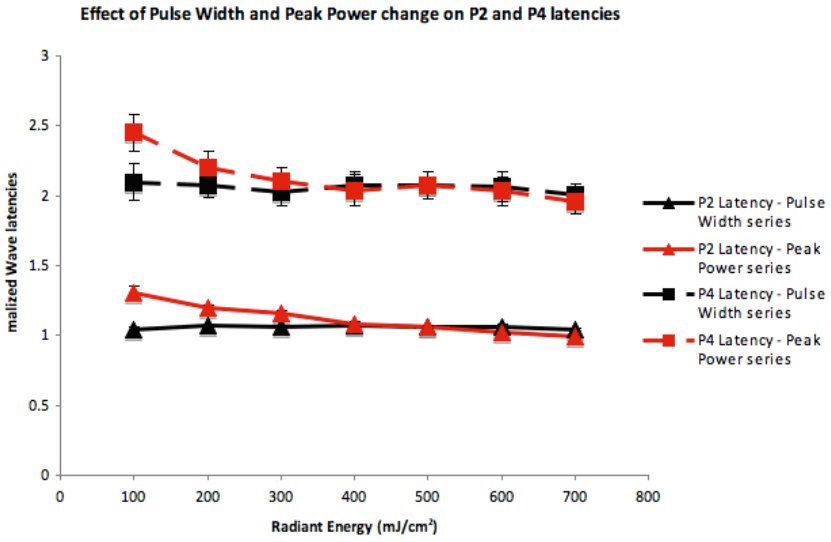


**Figure 18**. Effect of laser peak power series (red) and pulse width series (black) on the latency of P2 (full lines) and P4 (dotted lines). N=8

Statistical analyses show that the peak power has a significant effect on several parameters, including the amplitude and latency of P2, the total amplitude of the signal and the RMS energy of the signal ($p<0.05$). The pulse width, however, has no significant effect on any of the extracted parameters. The p-values obtained with the ANOVA tests on the effect of the different parametric series on the analyzed parameters are shown on figure 19.

| | Peak Power | Pulse Width | Wavelength at varying radiant energy | Wavelength at constant radiant energy | Pulse Rate |
|---|---|---|---|---|---|
| P2 amplitude | 0.001* | 0.893 | 0.090 | 0.852 | 0.001* |
| P4 amplitude | 0.519 | 0.994 | 0.999 | 0.977 | 0.878 |
| Total amplitude | 4.04E-05* | 0.978 | 0.090 | 0.820 | 3.77E-05* |
| P2 latency | 8.27E-12* | 0.674 | 0.303 | 0.747 | 2.34E-04* |
| P4 latency | 0.222 | 0.995 | 0.999 | 0.999 | 0.785 |
| RMS total | 0.004* | 0.988 | 0.999 | 0.999 | 0.930 |
| RMS of wave 2 | 0.159 | 0.989 | 0.999 | 0.999 | 0.951 |
| Percentage of energy in Wave 2 | 0.306 | 0.880 | 0.996 | 0.994 | 0.953 |

**Figure 19.** Table showing the p-values obtained after an ANOVA test for the effect of the different stimulation parameters on the analyzed signal parameters.

*Wavelength series*

We performed two types of studies into the effect of wavelength, 1) an alteration of wavelength from 1849 to 1865, but keeping the total energy deposited constant by varying the peak power and 1) varying the wavelength alone. In both conditions, no significant effect was found on any of the parameters (see figure 19). Figure 20 shows the measures of amplitude and latency of P2 and P4 at varying wavelengths in the two conditions.

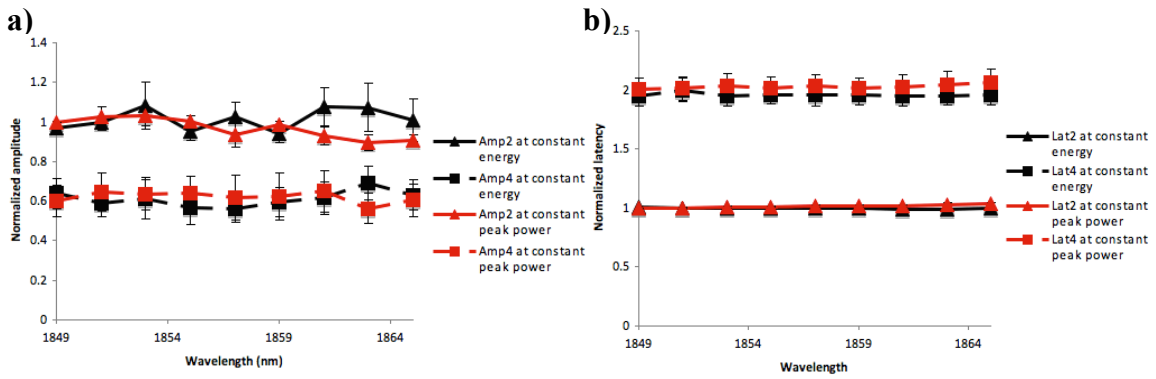


**Figure 20.** Effects of the wavelength series at constant radiant energy (in black) and constant peak power (in red) on a) the amplitudes of P2 and P4, and b) the latencies of P2 and P4. None of the effects are significant. N=8

*Pulse rate series*

The results of the pulse rate series between 3 and 63 Hz showed a significant effect of the pulse rate on the amplitude and latency of P2, and the total amplitude of the signal. The p-values are shown in figure 19, and the series are plotted for the amplitudes and latencies on figure 21.

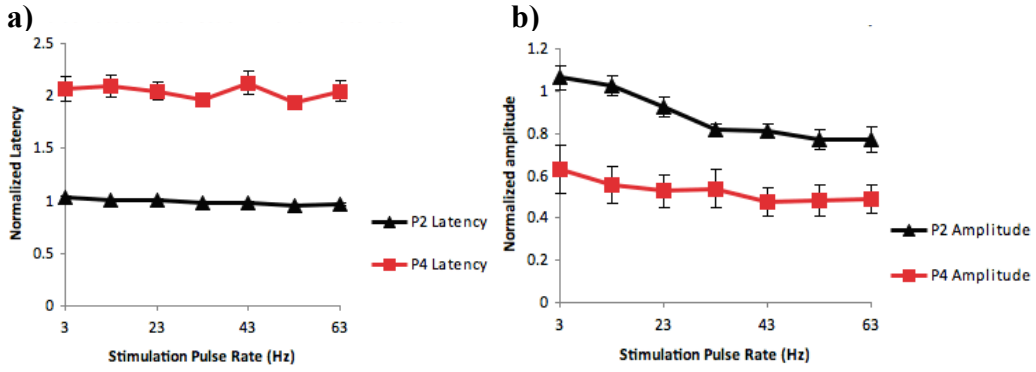


**Figure 21.** Effects of the pulse rate series on a) the amplitudes of P2 and P4, and b) the latencies of P2 and P4. The variation of the amplitude and latency of P2 are significant ($p<0.05$). N=8

## 3.5. IC Responses to INS

### 3.5.1. General

Recordings in the IC after INS on the CN showed that, above stimulation threshold, an increase in the spike numbers during the analyzed time window can be induced. An activation value is calculated in each case by averaging the spike counts. In most of the datasets, this activation is very broad across the electrodes, meaning that the entire ICCN is activated.

### 3.5.2. Parametric studies

The recordings performed in the IC by varying the stimulation parameters one by one showed a generally very broad activation, across nearly all the electrodes, as shown in the

example on figure 22. The main analysis is then done with the average value of activation across the electrodes for each level.

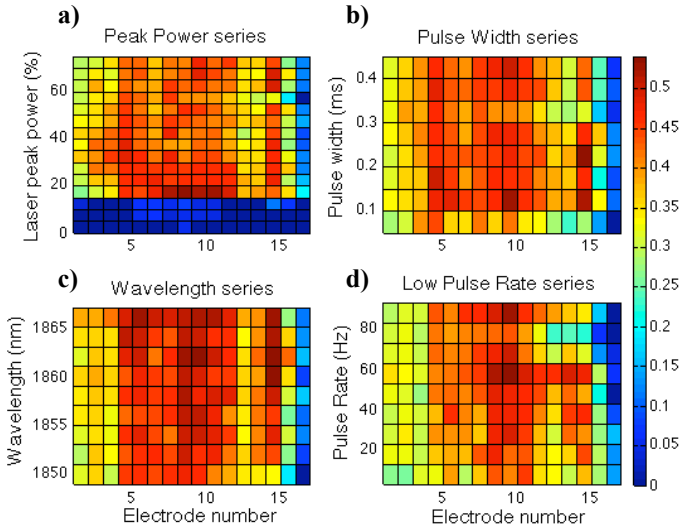


**Figure 22.** Example of a) laser peak power series, b) pulse width series, c) wavelength series and d) low pulse rate series obtained with IC recordings. The activation is very broad and non-frequency specific, which is confirmed statistically with the characteristic frequency ($p>0.05$). This extracted parameter does indeed not significantly vary with any of the stimulation parameters. The list of p-values is given on figure 24.

Unlike the ABR analyses, the reference laser peak power chosen here is 50%. The reason is that for pulse width series, the peak power of the laser is not increased up to 70% to avoid radiant energies of more than 750mJ/cm$^2$, which have been shown to induce tissue damage.[31] An average power level of 50% is then chosen as a safe stimulation level. The effects of varying different parameters on the average activity levels are shown on figure 23. Increasing the peak power of the laser to increase the radiant energy induces a significant change in the activity ($p<0.05$, see figure 24), particularly at peak powers lower than 30%, which was confirmed by a Tukey honest significance test. Varying the pulse width, wavelength and pulse rate has however no significant effect on the average activation level.

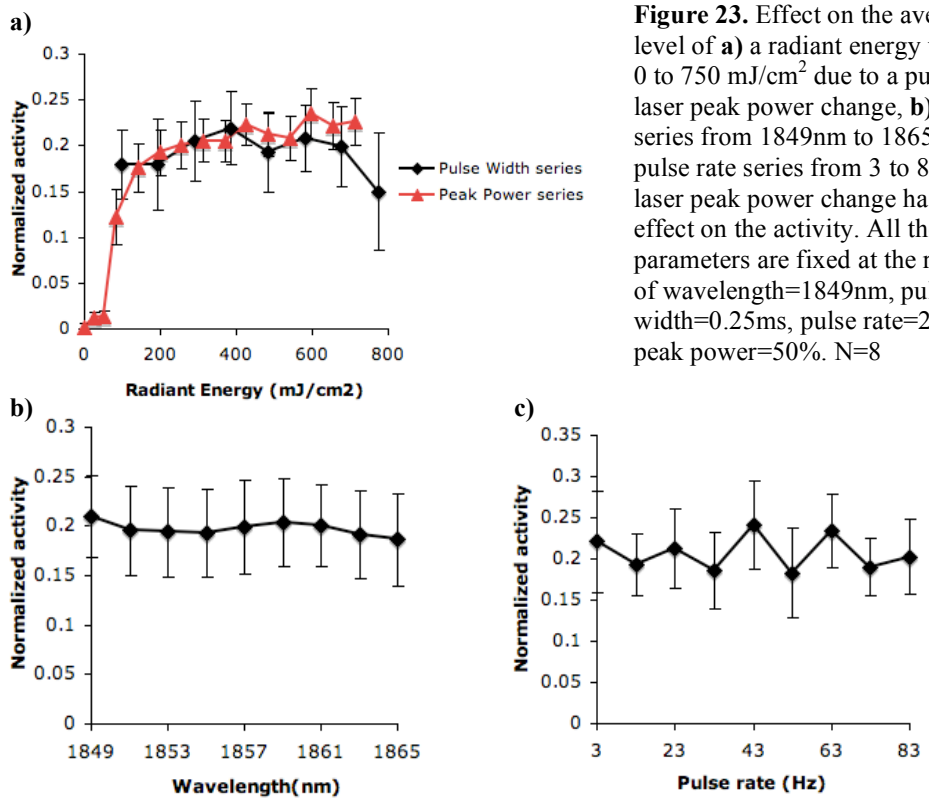


**Figure 23.** Effect on the average activity level of **a)** a radiant energy variation from 0 to 750 mJ/cm$^2$ due to a pulse width or laser peak power change, **b)** a wavelength series from 1849nm to 1865nm and **c)** a pulse rate series from 3 to 83 Hz. Only the laser peak power change has a significant effect on the activity. All the non-specified parameters are fixed at the reference values of wavelength=1849nm, pulse width=0.25ms, pulse rate=23Hz and laser peak power=50%. N=8

In addition to the analysis of the average activation across the electrodes for each parametric series, statistical analysis has been performed on the parameters extracted from the activation profiles showing for each value of a parametric series a two-dimensional profile with the spike counts at each peak power level and electrode. This means that those parameters, threshold, width of activation and characteristic frequency require a peak power series in addition to the parameter analyzed. They can then not be extracted from the peak power series alone, which explains the absence of p-value in the "Peak Power" column for these analyzed parameters on figure 24.

| | Pulse Width | Pulse Rate | Wavelength | Peak Power |
|---|---|---|---|---|
| Average activation across electrodes | 0.964 | 0.987 | 1 | 0* |
| Threshold[#] | 0.161 | 0.821 | 0.026* | |
| Width of activation[#] | 0.983 | 0.692 | 0.949 | |
| Characteristic frequency[#] | 0.987 | 0.999 | 0.998 | |

**Figure 24.** Table showing the p-values obtained after an ANOVA test for the effect of the different stimulation parameters on the analyzed signal parameters.
[#]: These parameters are calculated from a 2-dimensional map showing a laser peak power series in addition to the studied parameter.

The only significant effect of these profile parameters is an increase in threshold as the wavelength increases. This corresponds to a decrease in radiant energy from 483.5 mJ/cm$^2$ to 398.4 mJ/cm$^2$, but is also influenced by the change in absorbance, and hence in penetration depth of the infrared energy into the tissue. This effect can be seen on figure 25.

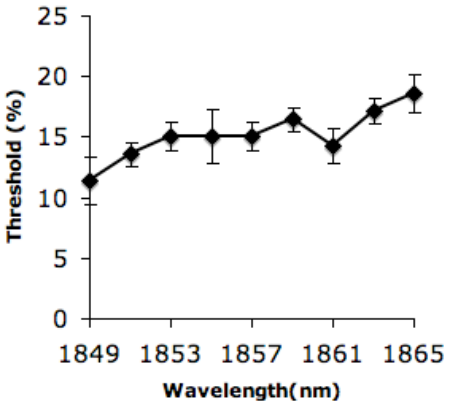


**Figure 25.** Effect of wavelength variation from 1849nm to 1865nm on the laser peak power threshold of activation in the IC. N=8

In addition to low pulse rate series, high pulse rate series were performed. By plotting the mean activation across the electrodes at a defined level of stimulation in a time dependent manner (average spike count per millisecond), the IC responses to high pulse rate stimulation can be compared between the different stimulation conditions, i.e. keeping the total energy constant by varying the pulse width or the peak power, or keeping the pulse width and peak power constant and letting the total energy vary with the pulse rate. Figure 26 shows an example of high pulse rate series at constant peak power and pulse width, which means the total energy brought to the tissue increases as the pulse width

increases from 100Hz to 500Hz. On this plot, the activation seems to follow the pulse rate, at least at 100Hz and 200Hz. At 500Hz, the total activation maximum is not higher than at lower pulse rates, but shows less variation. Finally, it can be seen that the pattern of activation changes a lot between 0 and 20ms, and then less for the rest of the run. This property is used in the following analysis, where the average spike count is calculated for each condition between 20 and 100ms as a measure of mean activation.

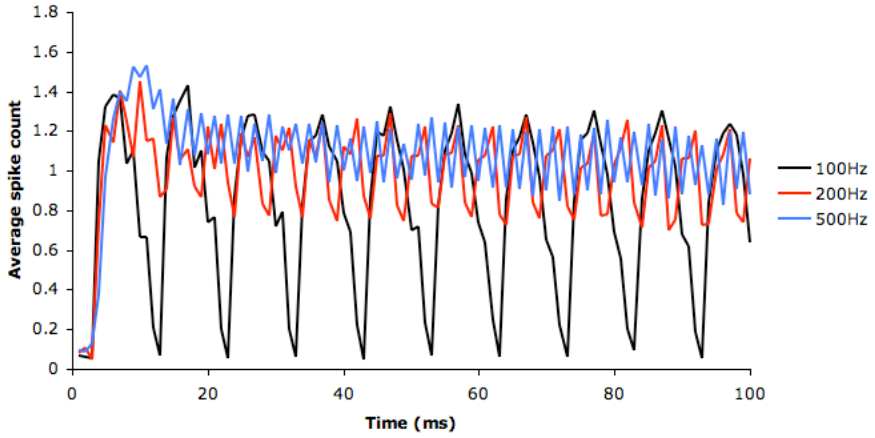


**Figure 26.** Example of average spike count at each millisecond during a high pulse rate series with a pulse width of 0.1ms, a laser peak power of 70% and a wavelength of 1849nm.

Figure 27 shows the average activation between 20ms and 100ms for pulse rates between 100Hz and 500Hz in the three different conditions described in the methods section of this report. A decrease in average activation can be seen as the pulse rate increases for the 'laser peak power variation' condition. In this case, the increase in total energy brought to the tissue when the pulse rate is increased is compensated by a decrease in peak power, to keep the total radiant energy brought to the tissue constant. This decrease in energy, not present in the other conditions where the peak power is not changed, reflects the major influence that the laser peak power has on the activation, already noticed in the peak power series at low pulse rate.

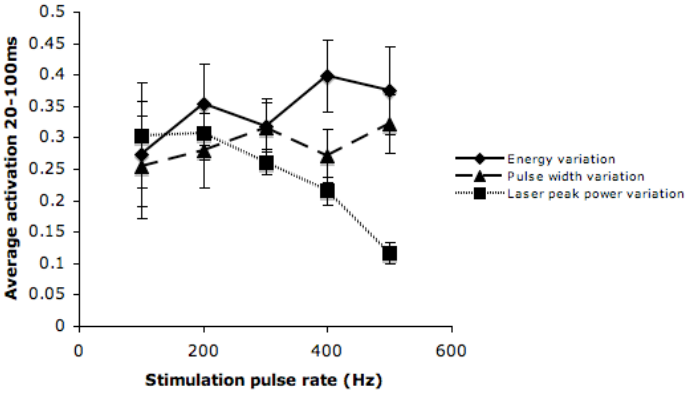


**Figure 27.** Average activation between 20ms and 100ms for high pulse rate series between 100Hz and 500Hz in the different conditions. N=6

### 3.6. Location studies

For the location studies, the goal was to investigate the dependence of the response on the location of the INS fiber during stimulation. The sites of placement of the fiber were defined with a 3-by-4 virtual grid (see figure 5). An example of ABR signals obtained at each of the 12 defined sites is shown on figure 28.

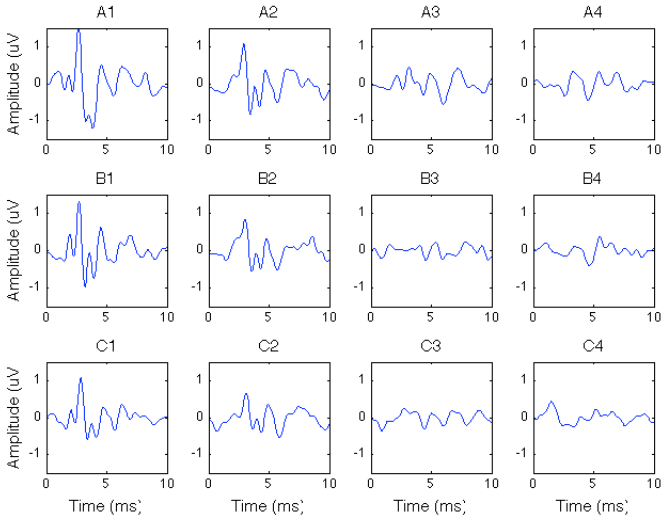


**Figure 28.** Example of ABR signals obtained with different stimulation sites on the CN surface following INS, with reference stimulation parameters.

Statistical tests were performed to determine if there is a location dependence along the two dimensions of the virtual grid (A-B-C and 1-2-3-4). The dimension 1 (A-B-C) corresponds to the rostral to caudal axis, and the dimension 2 corresponds to the lateral to medial axis. The effects of the ABR analyzed parameters, as well as the IC average spike count across the electrodes at a laser peak power of 50% were analyzed. Results show that the dimension 2 has a significant effect on all parameters except the ABR energy percentage in wave 2, whereas the dimension 1 has no significant effect on any of the parameters (see figure 32).

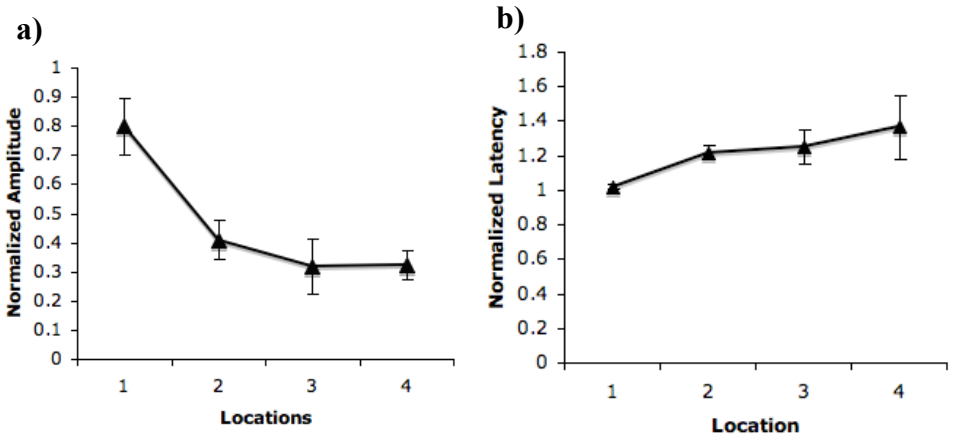


**Figure 29.** Effect of different locations from the lateral-to-medial axis (dimension 2) on a) the amplitude of P2 and b) the latency of P2 following INS. The different locations along that axis have a significant effect on both parameters. N=7

For the ABR parameters dependent on the presence of the different waves, the statistics were made only on the runs where a multipeaked ABR could be detected. The effect of the dimension 2 on the amplitude and latency of P2 are shown on figure 29. The percentage of presence of an ABR signal for locations along dimension 2 were calculated (see figure 30) and is clearly decreasing as the location moves from lateral to medial. The only ABR parameter independent of the presence of a multi-peaked response is the RMS energy of the total signal. Figure 31 shows the effect of different locations on the mean

energy of the signal. The dependence on dimension 2 (1-2-3-4) but not on dimension 1 (A-B-C) can clearly be seen.

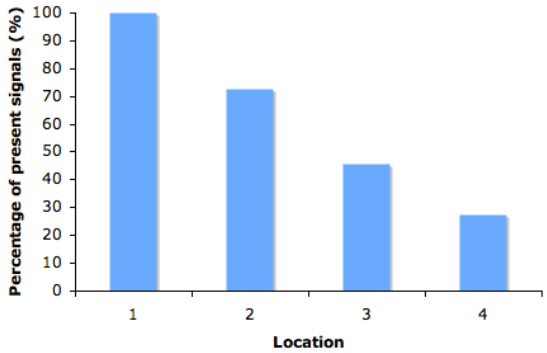


**Figure 30.** Percentage of presence of an ABR multi-peaked signal at different locations along the lateral-to-medial axis.

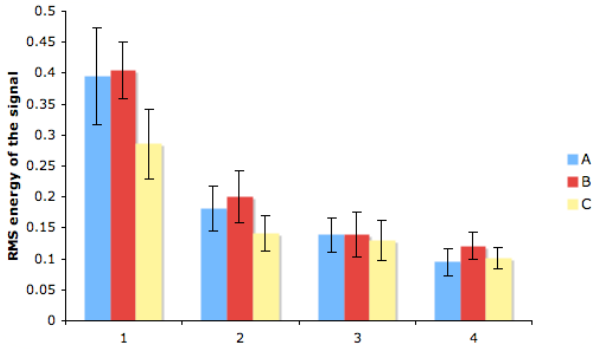


**Figure 31.** Averaged RMS values of the ABR signals at each stimulation site. Dimension 2 (1-2-3-4) has a significant effect, whereas dimension 1 (A-B-C) does not.

| | Effect of dimension 1 (A-B-C) | Effect of dimension 2 (1-2-3-4) |
|---|---|---|
| ABR P2 amplitude | 0.194 | 3.44E-4* |
| ABR P4 amplitude | 0.159 | 9.60E-3* |
| ABR Total amplitude | 0.174 | 1.63E-4* |
| ABR P2 latency | 0.897 | 1.53E-3* |
| ABR P4 latency | 0.840 | 4.09E-3* |
| ABR RMS total | 0.121 | 4.49E-13* |
| ABR RMS of wave 2 | 0.222 | 8.58E-7* |
| ABR Percentage of energy in Wave 2 | 0.856 | 0.103 |
| IC activation across electrodes at 50% laser power | 0.296 | 0.004* |

**Figure 32.** Table showing the p-values obtained after an ANOVA test for the effect of the different stimulation parameters on the analyzed signal parameters.

The effect of dimension 2 on the only IC analyzed parameter in this case, the average activation level across the electrodes at reference stimulation parameters, is shown on figure 33. The location along the lateral-to-medial axis has a significant effect ($p=0.004<0.05$), whereas the location along the rostral-to-caudal axis has no effect ($p=0.296>0.05$).

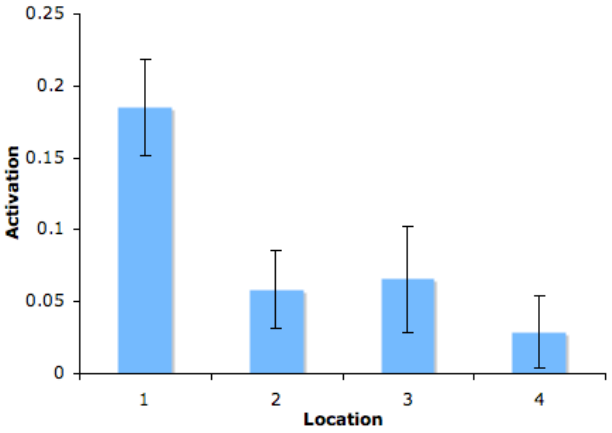


**Figure 33.** Effect of different locations from the lateral-to-medial axis on the IC averaged activation across the electrodes. N=7

Location studies with electrical stimulation have also been performed, in an attempt to compare the location dependence of INS and electrical stimulation. One example is shown in figure 34. The lateral-to-medial location dependence obtained with INS is not present here. However, the response still seems to be dependent on the location. In this example, we can see that locations B2, B3, C2 and C3 give the biggest ABRs. The responses in B4 and C4 show waveforms that are very different from ABRs and probably originate from other brain regions.

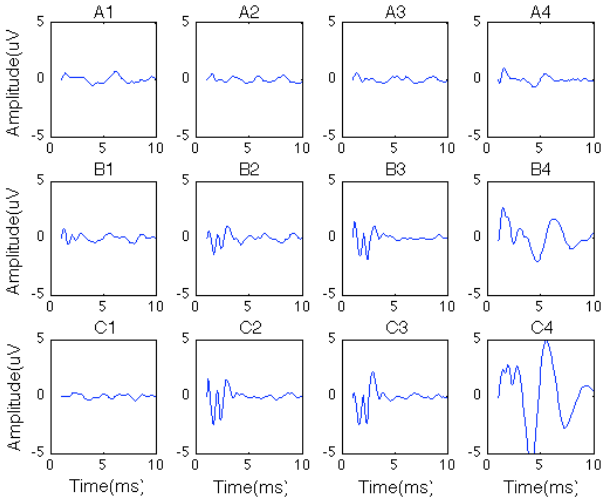


**Figure 34.** Example of electrically generated ABRs at different stimulation sites on the surface of the CN. The clear lateral-to-medial location dependence obtained with INS is not present here.

### 3.7. Acoustic noise artifact generated by the laser at the working parameters

At the working parameters of the laser, an acoustic artifact is generated by the INS laser[36]. This noise is a potential artifact in our data. Its parametric dependence is shown in figure 35.

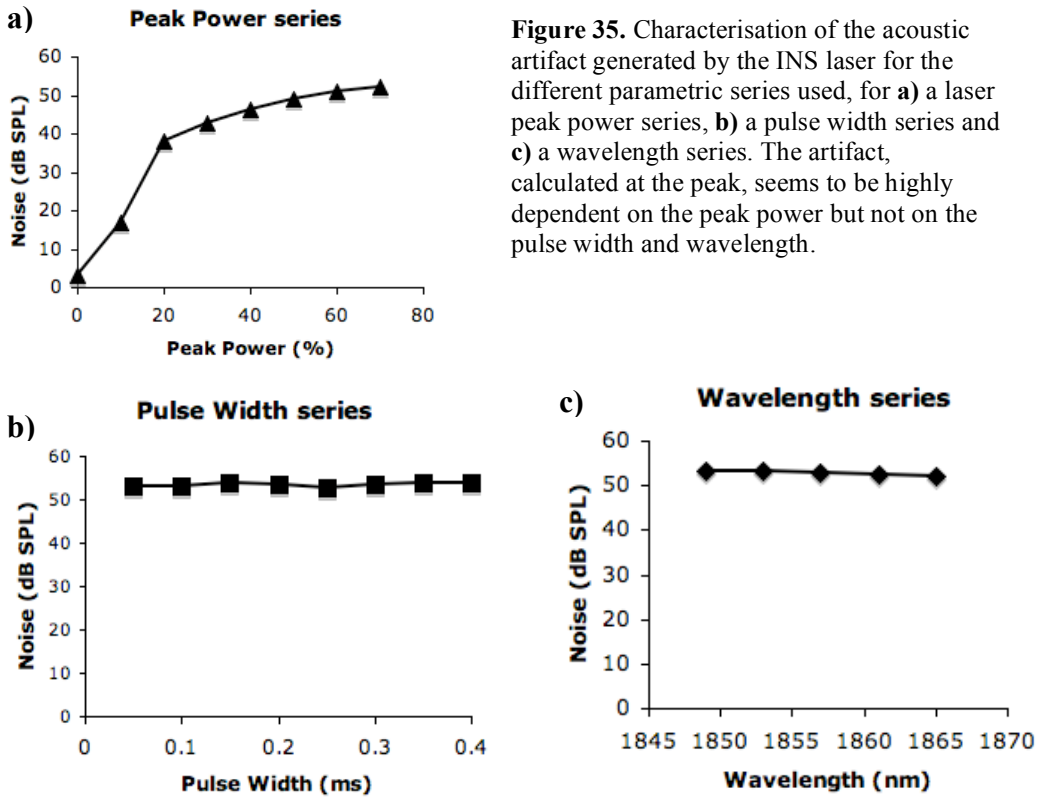


**Figure 35.** Characterisation of the acoustic artifact generated by the INS laser for the different parametric series used, for **a)** a laser peak power series, **b)** a pulse width series and **c)** a wavelength series. The artifact, calculated at the peak, seems to be highly dependent on the peak power but not on the pulse width and wavelength.

## 3.8. Deafening experiments

### 3.8.1. ABR

The parametric responses before and after deafening show a large effect of deafening. First, no peaks could be detected in the ABR signals obtained after deafening, which makes the analyses based on amplitudes and latencies of the peaks impossible. The following analyses then use the RMS energy of the total signal to compare the two conditions, as it is a measure independent of the presence of peaks.

Figure 37 shows the effect of deafening on ABR laser peak power, pulse width, pulse rate and wavelength series. For all steps of the 4 parametric series, the difference between before and after deafening is significant, except for the three first steps of the peak power series (see appendix 4).

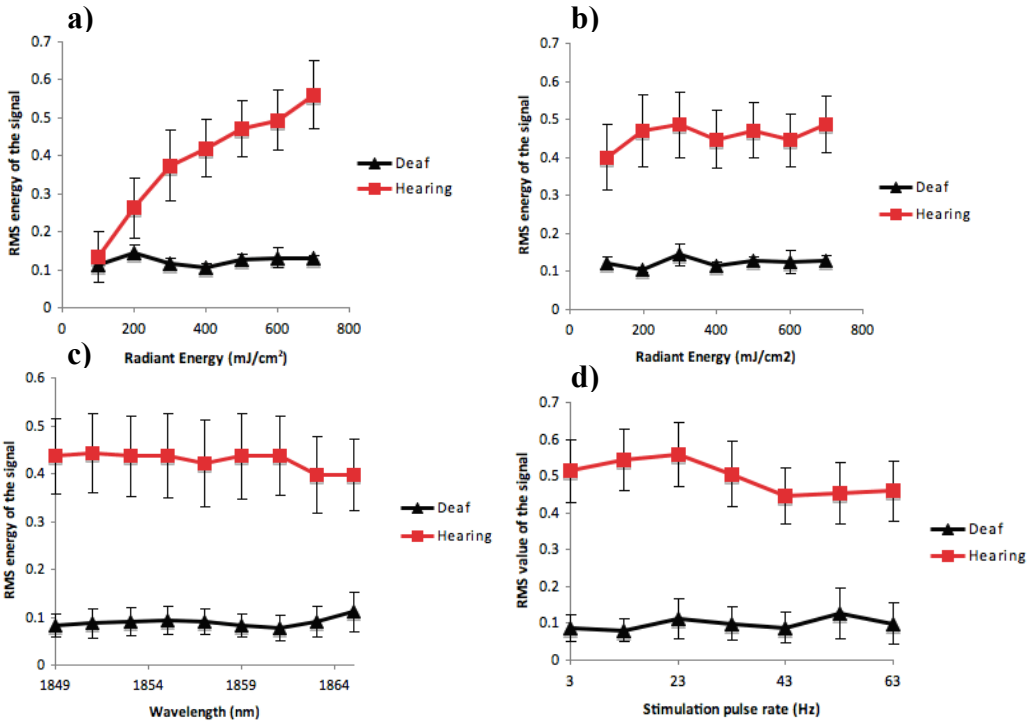


**Figure 37.** Effect of deafening on the RMS for **a)** a peak power series, **b)** a pulse width series, **c)** a wavelength series and **d)** a pulse rate series. N=3-8

The effect of deafening on all locations is shown on figure 38. Statistical analyses show a significant change between before and after deafening on the most lateral locations (A1 – B1 – C1), with p-values<0.05.

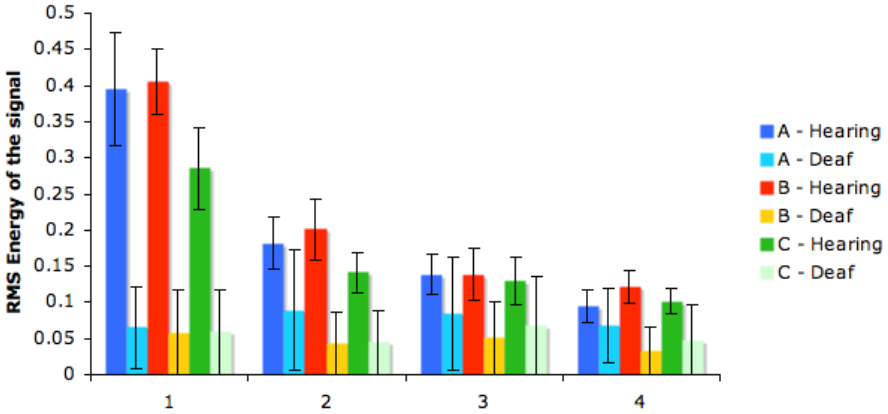


**Figure 38.** Effect of deafening on the RMS at each location on the virtual grid on the surface of the CN. N=3-8

### 3.8.2. IC

In the IC studies, the average spike count across the electrode array is used for the comparison between hearing and deaf subject data. First, parametric series before and after deafening were compared. The results show a significant decrease in activation after deafening for all different parametric series (see figure 39). The precise statistics can be found in appendix 4.

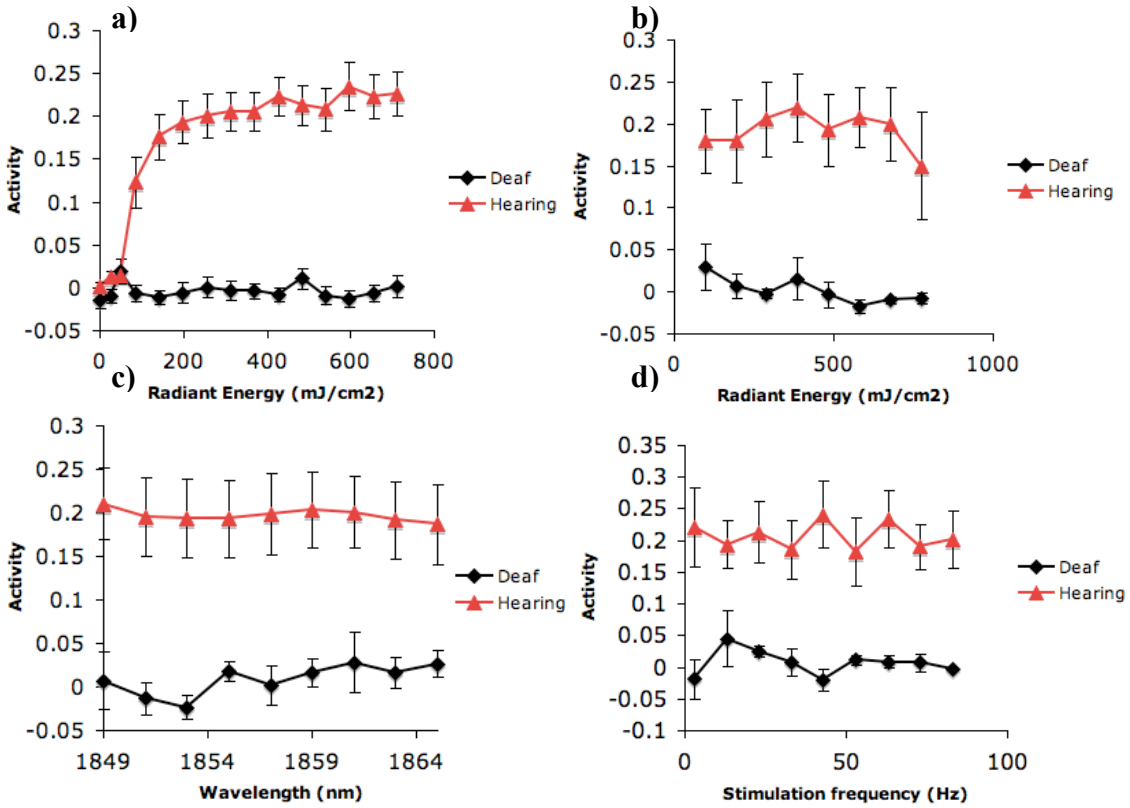


**Figure 39.** Effect of deafening on the average activation for **a)** a peak power series, **b)** a pulse width series, **c)** a wavelength series and d) a pulse rate series. N=3-8

Figure 40 shows the effects of deafening on all locations. This effect is significant for the data obtained at a more lateral location (location 1). At other locations, where the signal obtained before deafening is already weak, the effect of deafening is not significant.

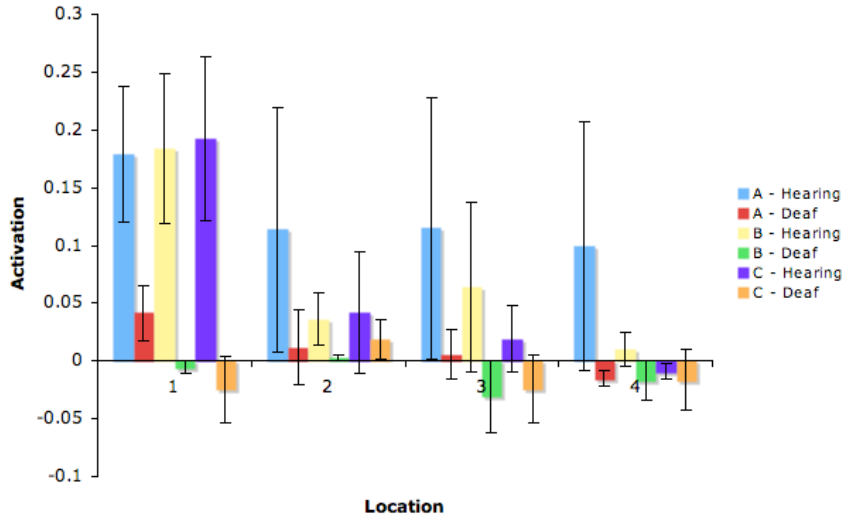


**Figure 40.** Effect of deafening on the average activation at each location on the virtual grid on the surface of the CN. N=3-8

### 3.8.3. Confirmation of the integrity of the central auditory system after deafening

After deafening by auditory nerve cutting, the integrity of the CN and the central auditory system has to be confirmed. For this purpose, ABRs are generated with electrical stimulation after deafening. Figure 36 shows an example of electrically generated ABR before and after deafening at approximately the same site that confirms the integrity of the central auditory system. This method is applied in each experiment after deafening, in order to ensure the validity of the data further acquired.

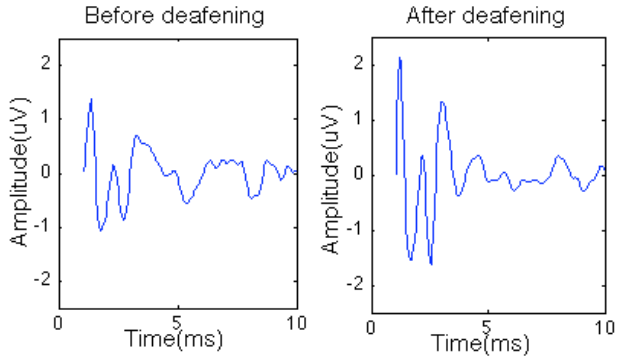


**Figure 36.** Example of electrically generated ABR before and after deafening by nerve cutting, confirming the integrity of the central auditory system.

The precise component of the acoustic artifact in the data is determined by doing the ABR and IC parametric and location studies after deafening of the animal and comparing them to data from hearing animals.

### 3.8.4. Control runs on the temporal bone and the 4th ventricle

Control runs have been performed by stimulating next to the CN to investigate whether a response is generated by stimulating these areas or not. These measures have been made before and after deafening. Results show a clear activation measured by both ABR and IC recordings after stimulation on the temporal bone. This activation disappears after deafening (figure 41).

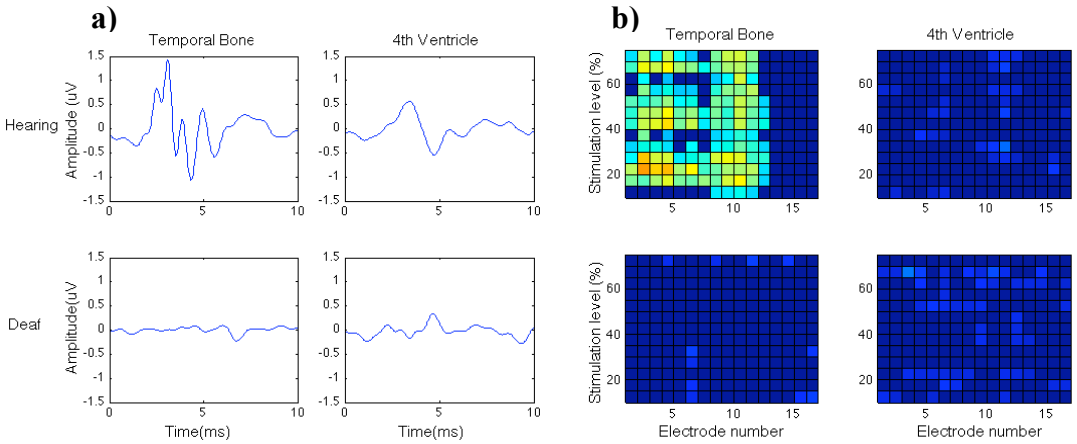


**Figure 41.** Examples of control runs for **a)** ABR and **b)** IC data on the temporal bone, directly lateral to the CN, and on the 4th ventricle, medial to the CN. An activation is clearly present during temporal bone stimulation, and disappears after deafening.

# 4. Discussion

General

The original question for this study was to use INS on the surface of a rodent CN to see if its auditory system could be activated by this means. The results show that a response can be recorded, both with ABR and IC recording methods, in normal hearing subjects. Then, we wanted to investigate what parameter of the energy delivered to the tissue has the greatest effect on the response, and if the location of stimulation on the CN surface is important.

Parametric studies

The parametric studies were performed by altering the peak power, the pulse width, the wavelength and the pulse rate of stimulation. We demonstrated that the peak power has the most significant effect on both ABR and IC recordings. The significant parameters of the ABR, like the amplitude of P2, the latency of P2, the RMS of the ABR signal and the IC average activation are all directly linked to the strength of the signal. It is known in human ABRs that as the stimulation level increases, the amplitudes of the waves increase whereas the latencies decrease, showing a quicker transmission of the stronger signal along the auditory pathway. [4]

Unlike in the peak power series, varying the pulse width showed no significant effect on any of the ABR or IC extracted parameters. Together, these two results show that the power of stimulation is more important than the amount of radiant energy brought to the tissue.

Because the wavelength also influences the power delivered to the tissue, this parameter could have been expected to have an effect on the responses that is similar to altering the laser's peak power. However, this is not the case, most likely because of the small range of wavelengths available with our laser (1849nm to 1865nm), which causes only a small energy variation. However, the absorbance of the tissue at different wavelength, estimated as the absorbance of water, varies significantly along this range of wavelengths, generating penetration depths of approximately 1100 to 600 μm.[39] This large variation in penetration depths may explain the shift in the activation threshold that can be seen on the IC data as the wavelength is changed. This might be due to a difference in number or type of cells activated at different penetration depths. If the change does not involve bushy cells, this may not have an effect on the ABR,

In the pulse rate series, a significant decrease in the amplitude of P2 was found as the pulse rate is increased from 3 to 63Hz. This effect could have different explanations. The simplest is that the activation level of the auditory pathway decreases as the stimulation pulse rate increases. It could also be due to the fact that the ABR signal can last for more than 10ms, and recordings at higher pulse rates would lead to superposition of successive signals, generating a waveform distortion in the signal that would decrease the measured amplitude of P2. Also, the fact that the ABR requires synchronous activity of a large number of neurons can cause this effect. At high pulse rates, there might be some residual activity from the previous pulse remaining at the beginning of the following pulse, preventing all the neurons to fire in a synchronous fashion. This would lead to a decrease of the amplitude of the signal's main wave, without necessarily a decrease in signal

energy. Considering that neither an energy nor activation level decrease has been found on the ABR and IC signals, a simple decrease of activity in the auditory system as the pulse rate increases is less likely to happen than a waveform distortion or asynchrony in activity, as previously explained.

Location studies

The second question asked in the characterization of INS is if the generated activity depends on the stimulation site on the CN surface. The results show that with INS, there is a statistically significant location dependence, the more lateral locations of the DCN generating a stronger activation, both with ABR and IC recordings. This characteristic does not seem to be present with electrical stimulation. If the electrical stimulation generates a significant level of current spread and the whole CN is activated, no matter where the electrode is, no obvious location dependence would be found. However, this explanation doesn't seem likely, because it would imply that the ABRs electrically generated at all the sites would be essentially the same, which is not the case in the dataset obtained. Therefore we can suggest that the activation mechanisms of ABR generation are different between electrical stimulation and INS.

Influence of the optophonic artifact on the response

The acoustic artifact generated during INS appears to be sufficient to activate the auditory system, since it can be as high as 50dB in most conditions, and the acoustic ABR thresholds of the subjects are all below 40dB. The presence of an artifact in the INS generated responses is then very likely. Several properties of the measured signals support this hypothesis. First, the waveforms of the ABRs generated with INS are much more similar to the acoustic ABRs than to the electrical ABRs with respect to peaks and latencies. If the ABRs were actually generated by INS, the first peak, generated roughly through activation of the auditory nerve, wouldn't appear in the signal.

Then, the comparison of the parametric series to the recorded acoustic artifacts shows similarities between this artifact and the variation of the parameters in the ABRs and IC recordings, which would be consistent with the hypothesis that the artifact influences the recorded data. Indeed, only the peak power has a significant effect both on the acoustic artifact and on the parameters extracted from the IC and ABR signals. The rapid increase in amplitude of P2 when the stimulation level is increased from 0% to 30% is also consistent with the artifact peak power series measurements.

As previously discussed, the recorded responses are stronger when the fiber is positioned close to the cochlea. Indeed, the strongest activations are measured when the fiber is placed at the most lateral sites. In this configuration, the fiber is very close to the temporal bone and the cochlea. As the stimulation location is moved more medially, the distance to the temporal bone is increased. As a result, the obtained responses are smaller or absent. These results are also consistent with an activation due to the acoustic artifact. Additionally, we can see on figure 41 that an ABR and IC response can be generated after stimulation on the temporal bone, which is a clear indication that the recorded activity is not the result of a CN direct stimulation.

The fact that the amplitudes of the ABRs generated with INS are comparable to the acoustically generated ABRs is also not consistent with a genuine laser stimulation of the neurons. Indeed, the basis of this study is that INS generates a very spatially specific stimulation that activates a small number of neurons. Therefore, we would expect an activation much smaller than after acoustic stimulation.

Another fact supporting the hypothesis of an optophonic artifact influencing the data is that in all cases, the IC activation is very wide and doesn't change when the parameters are varied. That is consistent with the fact that the noise generated by the laser is a click and not a tone, and hence would activate the whole range of frequencies at the same time, which is what we can observe in the IC recordings.

To confirm this hypothesis supported by all these characteristics of the recordings performed with hearing subjects, the same experiments were performed after deafening. Both in parametric and location experiments, in ABR and IC recordings, the INS generated signals are significantly reduced after deafening, although electrical ABRs can still be generated, confirming the integrity of the central auditory system. This result appears to confirm the acoustic artifact of INS activates the auditory system sufficiently strongly to cause ABR generation and IC responses.

Does INS optically activate the CN?

In the data obtained with ABRs and neurophysiological recordings in the IC, no significant responses in deafened subjects could be recorded. That does not necessarily mean that no stimulation was achieved. Indeed, with the recording methods used we were not able to detect the presence of local responses that may be very small in magnitude. ABR generation requires the activation of bushy cells, and it is known to require a strong synchronous activation. Since the goal here is anyway to stimulate a smaller area, hence a smaller number of neurons, it is not surprising that we cannot record any ABR signals in response to INS. The recordings in the IC do not require the neurons to fire synchronously, and are not dependent on the bushy cells activation. Indeed, the IC is an obligatory station for almost all the different auditory pathways activated, which means we could theoretically detect any activity traveling up the auditory pathway. However, it still requires an activation strong enough to travel up the auditory pathway to the IC. This might be why we were not able to record any response to INS stimulation in deafened subjects in the IC either. Moreover, it is known that the DCN is an important processing station of the sound, and that a limited number of fibers travel up to the IC. That might also be why no change in activity in the IC was recorded.

However, these results do not imply a total absence of neural activation. INS could activate neurons very locally, in stimulatory or inhibitory way, depending on the type of neurons it activates. The recording of this activity requires a single unit recording setup and the development of this new technique was not possible in the available timeframe.

# 5. Conclusion

Firstly, this study showed that no ABR could be generated with INS on a deafened subject because of an insufficient or non-synchronous activation of the bushy cells. This finding limits clinical use for ABIs using INS only, because the ABR is the intra-operative measure used to assess successful activation of the auditory system. Second, no responses could be recorded in the IC following INS either. This can be because the induced activation is too weak to travel up to the IC, or because the activated neurons are part of processing circuits in the DCN that do not have direct transmission fibers to the IC.

It is known that INS works in the peripheral auditory system and activates nerve fibers. The precise mechanism and the type of cells that can be activated or inhibited with INS has to be further studied in the central auditory system. INS might generate inhibition in the CN, as found in the somatosensory cortex[30], if the triggered layers of the CN contain mostly inhibitory cells. To understand the stimulation type that can be achieved, the functional anatomy of the CN has to be further understood.

The rodent model used in this study mimics the clinical situation, as only the DCN surface is surgically accessed. In ABI placement surgery, the direct visual access of the CN is also extremely limited. For research purposes, the other anatomical subdivisions of the CN could be stimulated to try to generate responses to INS. Accessing the AVCN and PVCN would require a different model and setup and a new surgical approach, but these structures are known to have more direct fibers going to the IC.

One way to record the local effects of INS would be to use single unit recordings. This technique is sensitive enough to detect weak responses, activatory or inhibitory, that might be generated in the processing circuits within the DCN. If a modulatory effect is found, INS could be used in a bimodal configuration to modulate electrical stimulation. For example, if INS generates an activatory effect, it could be used to facilitate stimulation by reducing the current threshold, which would decrease the current spread. INS pulses used in combination with subthreshold electrical stimulation could also generate activation. In this configuration, the INS spatial specificity and absence of artifact would be conserved. This is the focus of current research in the peripheral nervous system. [29]

The use of INS in the auditory system appears limited based on these results, however it is still an example of how novel stimulatory paradigms could be used in the development of neuroprostheses to improve the functional outcomes for patients with a variety of sensory deficits and have a significant impact on their quality of life.

## 6. Acknowledgements

I want to thank all the people who have helped and supported me throughout this project.
Fondation Bertarelli for providing the scholarship to make this project possible,
My Boston supervisors, Dr. Daniel J. Lee and Dr. M. Christian Brown, for their inspiration, guidance and support during this project,
My EPFL supervisors, Dr. Stephanie Lacour and Dr. Olaf Blanke, for their helpful advice and availability,
My laboratory colleague, Dr. Rohit Verma, for his great support, helpful discussions, thesis review and outstanding collaboration in general,
My colleague Dr. Nedim Durakovic for his precious advice and support, Kristen Babicz for her diligence and careful maintenance of the lab,
The EPL engineering team for their excellent and very prompt technical assistance, particularly Dr. Kenneth Hancock, Ishmael Stefanov and Evan Foss,
My family and friends, for their support and encouragements.

## 7. References

1. S.Blatrix, P.M. *Auditory Pathways*. Journey into the world of hearing 2009 - 2010 [cited 2011 14 Nov]; Available from: http://www.cochlea.org/en/spe/auditory-pathways-2.html.
2. Purves, D., *Neuroscience*. 4th ed2008, Sunderland, Mass.: Sinauer. xvii, 857, G-16, IC-7, I-29 p.
3. Clopton, B.M., J.A. Winfield, and F.J. Flammino, *Tonotopic organization: review and analysis.* Brain research, 1974. **76**(1): p. 1-20.
4. Hall, *New handbook for auditory evoked responses*2006.
5. Melcher, J.R., et al., *Generators of the brainstem auditory evoked potential in cat. II. Correlating lesion sites with waveform changes.* Hearing research, 1996. **93**(1-2): p. 28-51.
6. Lasky, R.E., et al., *Perinatal exposure to Aroclor 1254 impairs distortion product otoacoustic emissions (DPOAEs) in rats.* Toxicol Sci, 2002. **68**(2): p. 458-64.
7. Wilson, W.J. and F. Aghdasi, *The importance of pre-analysis windowing on auditory brainstem response fast Fourier transform analysis.* Scand Audiol, 2001. **30**(1): p. 3-12.
8. Richter, C.P., et al., *Spread of cochlear excitation during stimulation with pulsed infrared radiation: inferior colliculus measurements.* Journal of neural engineering, 2011. **8**(5): p. 056006.
9. Snyder, R.L., J.A. Bierer, and J.C. Middlebrooks, *Topographic spread of inferior colliculus activation in response to acoustic and intracochlear electric stimulation.* J Assoc Res Otolaryngol, 2004. **5**(3): p. 305-22.
10. Barsz, K., W.W. Wilson, and J.P. Walton, *Reorganization of receptive fields following hearing loss in inferior colliculus neurons.* Neuroscience, 2007. **147**(2): p. 532-45.
11. Snyder, R.L. and D.G. Sinex, *Immediate changes in tuning of inferior colliculus neurons following acute lesions of cat spiral ganglion.* Journal of neurophysiology, 2002. **87**(1): p. 434-52.
12. Shivdasani, M.N., et al., *Inferior colliculus responses to multichannel microstimulation of the ventral cochlear nucleus: implications for auditory brain stem implants.* Journal of neurophysiology, 2008. **99**(1): p. 1-13.
13. Bond, M., et al., *The effectiveness and cost-effectiveness of cochlear implants for severe to profound deafness in children and adults: a systematic review and economic model.* Health Technol Assess, 2009. **13**(44): p. 1-330.
14. Colletti, V., et al., *Progress in restoration of hearing with the auditory brainstem implant.* Progress in brain research, 2009. **175**: p. 333-45.
15. Evans, G.R., S.K. Lloyd, and R.T. Ramsden, *Neurofibromatosis type 2.* Adv Otorhinolaryngol, 2011. **70**: p. 91-8.
16. McCreery, D.B., *Cochlear nucleus auditory prostheses.* Hear Res, 2008. **242**(1-2): p. 64-73.
17. Sennaroglu, L., et al., *Auditory brainstem implantation in children and non-neurofibromatosis type 2 patients: a consensus statement.* Otol Neurotol, 2011. **32**(2): p. 187-91.

18. Shannon, R.V., et al., *Threshold-distance measures from electrical stimulation of human brainstem.* IEEE transactions on rehabilitation engineering : a publication of the IEEE Engineering in Medicine and Biology Society, 1997. **5**(1): p. 70-4.
19. Otto, S.R., et al., *The multichannel auditory brain stem implant: performance in twenty patients.* Otolaryngol Head Neck Surg, 1998. **118**(3 Pt 1): p. 291-303.
20. Otto, S.R., et al., *Audiologic outcomes with the penetrating electrode auditory brainstem implant.* Otology & neurotology : official publication of the American Otological Society, American Neurotology Society [and] European Academy of Otology and Neurotology, 2008. **29**(8): p. 1147-54.
21. Wells, J., et al., *Optical stimulation of neural tissue in vivo.* Opt Lett, 2005. **30**(5): p. 504-6.
22. Wells, J., et al., *Pulsed laser versus electrical energy for peripheral nerve stimulation.* J Neurosci Methods, 2007. **163**(2): p. 326-37.
23. Shapiro, M.G., et al., *Infrared light excites cells by changing their electrical capacitance.* Nat Commun, 2012. **3**: p. 736.
24. Wells, J., et al., *Biophysical mechanisms of transient optical stimulation of peripheral nerve.* Biophys J, 2007. **93**(7): p. 2567-80.
25. Jenkins, M.W., et al., *Optical pacing of the embryonic heart.* Nat Photonics, 2010. **4**: p. 623-626.
26. Teudt, I.U., et al., *Optical stimulation of the facial nerve: a new monitoring technique?* The Laryngoscope, 2007. **117**(9): p. 1641-7.
27. Rajguru, S.M., et al., *Infrared photostimulation of the crista ampullaris.* J Physiol, 2011. **589**(Pt 6): p. 1283-94.
28. Fried, N.M., et al., *Laser stimulation of the cavernous nerves in the rat prostate, in vivo: optimization of wavelength, pulse energy, and pulse repetition rate.* Conf Proc IEEE Eng Med Biol Soc, 2008. **2008**: p. 2777-80.
29. Duke, A.R., et al., *Combined optical and electrical stimulation of neural tissue in vivo.* Journal of biomedical optics, 2009. **14**(6): p. 060501.
30. Cayce, J.M., et al., *Pulsed infrared light alters neural activity in rat somatosensory cortex in vivo.* Neuroimage, 2011. **57**(1): p. 155-66.
31. Wells, J.D., et al., *Optically mediated nerve stimulation: Identification of injury thresholds.* Lasers Surg Med, 2007. **39**(6): p. 513-26.
32. Izzo, A.D., et al., *Optical parameter variability in laser nerve stimulation: a study of pulse duration, repetition rate, and wavelength*. IEEE transactions on bio-medical engineering, 2007. **54**(6 Pt 1): p. 1108-14.
33. Littlefield, P.D., et al., *Laser stimulation of single auditory nerve fibers.* The Laryngoscope, 2010. **120**(10): p. 2071-82.
34. Izzo, A.D., et al., *Selectivity of neural stimulation in the auditory system: a comparison of optic and electric stimuli.* Journal of biomedical optics, 2007. **12**(2): p. 021008.
35. Izzo, A.D., et al., *Laser stimulation of the auditory nerve.* Lasers Surg Med, 2006. **38**(8): p. 745-53.
36. Teudt, I.U., et al., *Acoustic events and "optophonic" cochlear responses induced by pulsed near-infrared laser*. IEEE transactions on bio-medical engineering, 2011. **58**(6): p. 1648-55.
37. Richter, C.P., et al., *Optical stimulation of auditory neurons: effects of acute and chronic deafening.* Hearing research, 2008. **242**(1-2): p. 42-51.
38. Hackney, C.M., K.K. Osen, and J. Kolston, *Anatomy of the cochlear nuclear complex of guinea pig.* Anat Embryol (Berl), 1990. **182**(2): p. 123-49.
39. Walsh, J.T., Jr. and J.P. Cummings, *Effect of the dynamic optical properties of water on midinfrared laser ablation.* Lasers Surg Med, 1994. **15**(3): p. 295-305.
40. Laukli, E. and I.W. Mair, *Early auditory-evoked responses: spectral content.* Audiology, 1981. **20**(6): p. 453-64.
41. Wilson, W.J., *The relationship between the auditory brain-stem response and its reconstructed waveforms following discrete wavelet transformation.* Clin Neurophysiol, 2004. **115**(5): p. 1129-39.
42. Lim, H.H. and D.J. Anderson, *Auditory cortical responses to electrical stimulation of the inferior colliculus: implications for an auditory midbrain implant.* J Neurophysiol, 2006. **96**(3): p. 975-88.

## Appendix 1: ABR experiments stimulation parameters

**Energy Series by varying laser peak power and pulse width**

| run | Peak power | Pulse rate | Pulse width | Radiant energy | Wavelength |
|---|---|---|---|---|---|
| | 51.5 | 23 | 0.05 | | 1849 |
| | 29.5 | 23 | 0.1 | | 1849 |
| | 22.1 | 23 | 0.15 | | 1849 |
| | 18.5 | 23 | 0.2 | 100 | 1849 |
| | 16.3 | 23 | 0.25 | | 1849 |
| | 14.8 | 23 | 0.3 | | 1849 |
| | 13.8 | 23 | 0.35 | | 1849 |
| | 51.5 | 23 | 0.1 | | 1849 |
| | 36.8 | 23 | 0.15 | | 1849 |
| | 29.5 | 23 | 0.2 | | 1849 |
| | 25.1 | 23 | 0.25 | 200 | 1849 |
| | 22.1 | 23 | 0.3 | | 1849 |
| | 20.1 | 23 | 0.35 | | 1849 |
| | 18.5 | 23 | 0.4 | | 1849 |
| | 73.4 | 23 | 0.1 | | 1849 |
| | 51.5 | 23 | 0.15 | | 1849 |
| | 40.5 | 23 | 0.2 | | 1849 |
| | 33.9 | 23 | 0.25 | 300 | 1849 |
| | 29.5 | 23 | 0.3 | | 1849 |
| | 26.3 | 23 | 0.35 | | 1849 |
| | 24 | 23 | 0.4 | | 1849 |
| | 66.1 | 23 | 0.15 | | 1849 |
| | 51.5 | 23 | 0.2 | | 1849 |
| | 42.7 | 23 | 0.25 | | 1849 |
| | 36.8 | 23 | 0.3 | 400 | 1849 |
| | 32.6 | 23 | 0.35 | | 1849 |
| | 29.5 | 23 | 0.4 | | 1849 |
| | 27 | 23 | 0.45 | | 1849 |
| | 62.4 | 23 | 0.2 | | 1849 |
| | 51.5 | 23 | 0.25 | | 1849 |
| | 44.1 | 23 | 0.3 | | 1849 |
| | 38.9 | 23 | 0.35 | 500 | 1849 |
| | 35 | 23 | 0.4 | | 1849 |
| | 31.9 | 23 | 0.45 | | 1849 |
| | 29.5 | 23 | 0.5 | | 1849 |
| | 73.4 | 23 | 0.2 | | 1849 |
| | 60.2 | 23 | 0.25 | | 1849 |
| | 51.5 | 23 | 0.3 | | 1849 |
| | 45.2 | 23 | 0.35 | 600 | 1849 |
| | 40.5 | 23 | 0.4 | | 1849 |
| | 36.8 | 23 | 0.45 | | 1849 |
| | 33.9 | 23 | 0.5 | | 1849 |
| | 69 | 23 | 0.25 | | 1849 |
| | 58.8 | 23 | 0.3 | | 1849 |
| | 51.5 | 23 | 0.35 | | 1849 |
| | 46 | 23 | 0.4 | 700 | 1849 |
| | 41.7 | 23 | 0.45 | | 1849 |
| | 38.3 | 23 | 0.5 | | 1849 |
| | 35.5 | 23 | 0.55 | | 1849 |

**Wavelength series at constant energy**

| run | Peak power | Pulse rate | Radiant Energy | Wavelength |
|---|---|---|---|---|
| | 60 | 23 | 597 | 1849 |
| | 61.2 | 23 | 597 | 1851 |
| | 62.4 | 23 | 597 | 1853 |
| | 63.7 | 23 | 597 | 1855 |
| | 65.1 | 23 | 597 | 1857 |
| | 66.5 | 23 | 597 | 1859 |
| | 68 | 23 | 597 | 1861 |
| | 69.6 | 23 | 597 | 1863 |
| | 71.2 | 23 | 597 | 1865 |

**Energy Series by varying wavelength**

| | | | | |
|---|---|---|---|---|
| | 60 | 23 | 597 | 1849 |
| | 60 | 23 | 584.1 | 1851 |
| | 60 | 23 | 571 | 1853 |
| | 60 | 23 | 557.8 | 1855 |
| | 60 | 23 | 544.7 | 1857 |
| | 60 | 23 | 531.6 | 1859 |
| | 60 | 23 | 518.4 | 1861 |
| | 60 | 23 | 505.3 | 1863 |
| | 60 | 23 | 492.1 | 1865 |

**Pulse Rate series**

| | | | | |
|---|---|---|---|---|
| | 70 | 3 | 711 | 1849 |
| | 70 | 13 | 711 | 1849 |
| | 70 | 23 | 711 | 1849 |
| | 70 | 33 | 711 | 1849 |
| | 70 | 43 | 711 | 1849 |
| | 70 | 53 | 711 | 1849 |
| | 70 | 63 | 711 | 1849 |
| | 70 | 73 | 711 | 1849 |
| | 70 | 83 | 711 | 1849 |

**Location study**

| | | | | | Location |
|---|---|---|---|---|---|
| | 70 | 23 | 711 | 1849 | A1 |
| | 70 | 23 | 711 | 1849 | A2 |
| | 70 | 23 | 711 | 1849 | A3 |
| | 70 | 23 | 711 | 1849 | A4 |
| | 70 | 23 | 711 | 1849 | B1 |
| | 70 | 23 | 711 | 1849 | B2 |
| | 70 | 23 | 711 | 1849 | B3 |
| | 70 | 23 | 711 | 1849 | B4 |
| | 70 | 23 | 711 | 1849 | C1 |
| | 70 | 23 | 711 | 1849 | C2 |
| | 70 | 23 | 711 | 1849 | C3 |
| | 70 | 23 | 711 | 1849 | C4 |

## Appendix 2: IC experiments stimulation parameters

| run | Pulse Rate series (low) | | | | | | | | | |
|---|---|---|---|---|---|---|---|---|---|---|
| | 0 to 70 | 0.25 | 3 | 1849 | | | | | | |
| | 0 to 70 | 0.25 | 13 | 1849 | | | | | | |
| | 0 to 70 | 0.25 | 23 | 1849 | | | | | | |
| | 0 to 70 | 0.25 | 33 | 1849 | | | | | | |
| | 0 to 70 | 0.25 | 43 | 1849 | | **INS** | | | | |
| | 0 to 70 | 0.25 | 53 | 1849 | | **Location** | | | | |
| | 0 to 70 | 0.25 | 63 | 1849 | | **IC** | 1 | 2 | 3 | 4 |
| | 0 to 70 | 0.25 | 73 | 1849 | | A | | | | |
| | 0 to 70 | 0.25 | 83 | 1849 | | B | | | | |
| | **Wavelength series** | | | | | C | | | | |
| | 0 to 70 | 0.25 | 23 | 1849 | | | | | | |
| | 0 to 70 | 0.25 | 23 | 1851 | | **ABR** | 1 | 2 | 3 | 4 |
| | 0 to 70 | 0.25 | 23 | 1853 | | A | | | | |
| | 0 to 70 | 0.25 | 23 | 1855 | | B | | | | |
| | 0 to 70 | 0.25 | 23 | 1857 | | C | | | | |
| | 0 to 70 | 0.25 | 23 | 1859 | | | | | | |
| | 0 to 70 | 0.25 | 23 | 1861 | | | | | | |
| | 0 to 70 | 0.25 | 23 | 1863 | | **Electrical** | | | | |
| | 0 to 70 | 0.25 | 23 | 1865 | | **Location** | | | | |
| | **Pulse Width series** | | | | | **IC** | 1 | 2 | 3 | 4 |
| | 0 to 70 | 0.05 | 23 | 1849 | | A | | | | |
| | 0 to 70 | 0.1 | 23 | 1849 | | B | | | | |
| | 0 to 70 | 0.15 | 23 | 1849 | | C | | | | |
| | 0 to 70 | 0.2 | 23 | 1849 | | | | | | |
| | 0 to 70 | 0.25 | 23 | 1849 | | **ABR** | 1 | 2 | 3 | 4 |
| | 0 to 60 | 0.3 | 23 | 1849 | | A | | | | |
| | 0 to 55 | 0.35 | 23 | 1849 | | B | | | | |
| | 0 to 45 | 0.4 | 23 | 1849 | | C | | | | |

| | High pulse rate (pulse width change) | | | | |
|---|---|---|---|---|---|
| | % | PW | PR | WL | duration |
| | 0 to 70 | 0.25 | 100 | 1849 | 100 ms |
| | 0 to 70 | 0.12 | 200 | 1849 | 100 ms |
| | 0 to 70 | 0.08 | 300 | 1849 | 100 ms |
| | 0 to 70 | 0.06 | 400 | 1849 | 100 ms |
| | 0 to 70 | 0.05 | 500 | 1849 | 100 ms |
| | **High pulse rate (energy change)** | | | | |
| | 0 to 70 | 0.1 | 100 | 1849 | 100 ms |
| | 0 to 70 | 0.1 | 200 | 1849 | 100 ms |
| | 0 to 70 | 0.1 | 300 | 1849 | 100 ms |
| | 0 to 70 | 0.1 | 400 | 1849 | 100 ms |
| | 0 to 70 | 0.1 | 500 | 1849 | 100 ms |
| | **High pulse rate (peak power change)** | | | | |
| | 0 to 70 | 0.1 | 100 | 1849 | 100 ms |
| | 0 to 35 | 0.1 | 200 | 1849 | 100 ms |
| | 0 to 23.33 | 0.1 | 300 | 1849 | 100 ms |
| | 0 to 17.5 | 0.1 | 400 | 1849 | 100 ms |
| | 0 to 14 | 0.1 | 500 | 1849 | 100 ms |

**Appendix 3: Model of the cochlear nucleus: Images and measurements**

2-dimensional views of the CN from a caudal, dorsal and lateral point of view

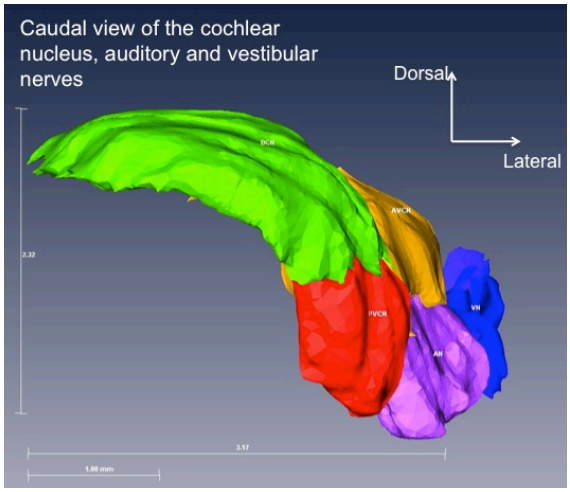


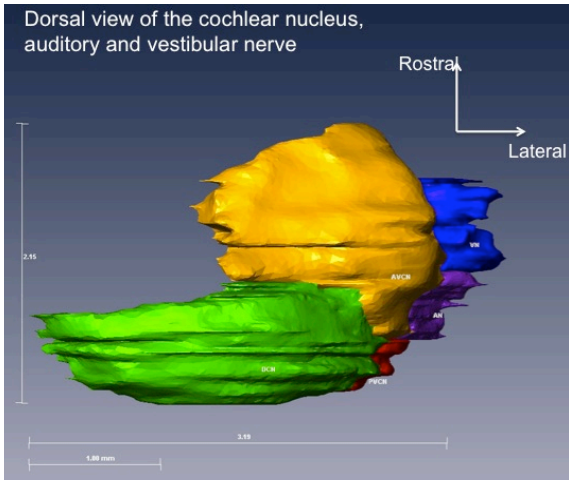


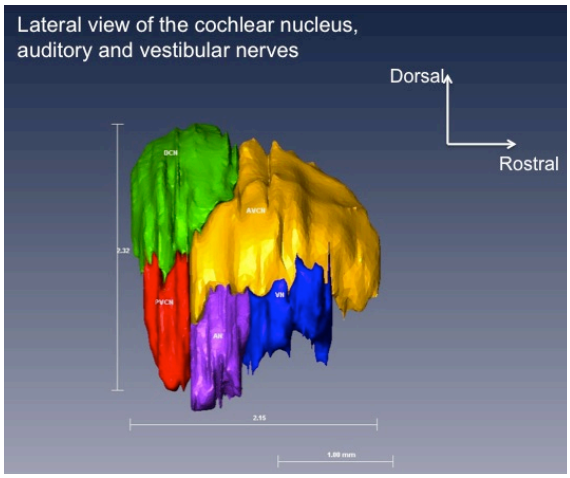


Measurements from the different anatomical subdivisions of the CN

| | DCN | AVCN | PVCN | CN |
|---|---|---|---|---|
| Distance along the medio-lateral axis | 2.79mm | 1.98mm | 1.31mm | 3.17mm |
| Distance along the rostro-caudal axis | 0.93mm | 1.66mm | 0.41mm | 2.15mm |
| Distance along the dorso-ventral axis | 1.47mm | 2.12mm | 1.71mm | 2.32mm |
| Estimated volume | 0.628mm$^3$ | 1.209mm$^3$ | 0.247mm$^3$ | 2.084mm$^3$ |

**Appendix 4: Statistical analyses results after deafening**

Shown below are the p-values obtained with a one-way ANOVA test for the comparison of the averages of the obtained values before and after deafening, for each condition. The statistics were calculated on the RMS energy of the total signal for the ABR data and on the average activation across the electrodes for the IC data. The significant values ($p<0.05$) are highlighted in light blue.

ABR parametric studies data

*Peak power series*

| Radiant energy (mJ/cm$^2$) | 100 | 200 | 300 | 400 | 500 | 600 | 700 |
|---|---|---|---|---|---|---|---|
| P-value | 0.847 | 0.379 | 0.107 | 0.029 | 0.015 | 0.019 | 0.015 |

*Pulse width series*

| Radiant energy (mJ/cm$^2$) | 100 | 200 | 300 | 400 | 500 | 600 | 700 |
|---|---|---|---|---|---|---|---|
| P-value | 0.077 | 0.043 | 0.037 | 0.023 | 0.015 | 0.017 | 0.017 |

*Wavelength series (A: at constant radiant energy, B: at constant peak power)*

| Wavelength (nm) | 1849 | 1851 | 1853 | 1855 | 1857 | 1859 | 1861 | 1863 | 1865 |
|---|---|---|---|---|---|---|---|---|---|
| P-value – A | 0.004 | 0.003 | 0.002 | 0.005 | 0.002 | 0.006 | 5.75E-4 | 7.31E-4 | 8.8E-4 |
| P-value – B | 0.005 | 0.007 | 0.008 | 0.009 | 0.014 | 0.009 | 0.005 | 0.011 | 0.013 |

*Pulse rate series*

| Pulse rate (Hz) | 3 | 13 | 23 | 33 | 43 | 53 | 63 |
|---|---|---|---|---|---|---|---|
| P-value | 0.016 | 0.008 | 0.004 | 0.025 | 0.015 | 0.049 | 0.024 |

ABR location studies data

*All locations*

| Location | A1 | A2 | A3 | A4 | B1 | B2 | B3 | B4 | C1 | C2 | C3 | C4 |
|---|---|---|---|---|---|---|---|---|---|---|---|---|
| P-value | 0.023 | 0.203 | 0.358 | 0.531 | 0.001 | 0.095 | 0.457 | 0.246 | 0.039 | 0.116 | 0.443 | 0.272 |

*Locations along dimension 2 (lateral-to-medial axis)*

| Location | 1 | 2 | 3 | 4 |
|---|---|---|---|---|
| P-value | 5.30E-06 | 0.007 | 0.129 | 0.078 |

IC parametric studies data

*Peak power series*

| Peak power (%) | 0 | 5 | 10 | 15 | 20 | 25 | 30 | 35 |
|---|---|---|---|---|---|---|---|---|
| P-value | 0.115 | 0.033 | 0.697 | 0.004 | 1.46E-5 | 3.33E-6 | 5.28E-6 | 3.23E-7 |
| Peak power (%) | 40 | 45 | 50 | 55 | 60 | 65 | 70 | |
| P-value | 1.71E-7 | 2.99E-8 | 1.04E-6 | 5.14E-7 | 4.10E-7 | 3.96E-7 | 6.88E-7 | |

*Pulse width series*

| Pulse width (ms) | 0.05 | 0.1 | 0.15 | 0.2 | 0.25 | 0.3 | 0.35 | 0.4 |
|---|---|---|---|---|---|---|---|---|
| P-value | 0.015 | 0.022 | 0.005 | 0.004 | 0.006 | 8.10E-4 | 0.004 | 0.082 |

*Wavelength series*

| Wavelength (nm) | 1849 | 1851 | 1853 | 1855 | 1857 | 1859 | 1861 | 1863 | 1865 |
|---|---|---|---|---|---|---|---|---|---|
| P-value | 0.005 | 0.005 | 0.004 | 0.014 | 0.010 | 0.009 | 0.013 | 0.012 | 0.024 |

*Pulse rate series*

| Pulse rate (Hz) | 3 | 13 | 23 | 33 | 43 | 53 | 63 | 73 | 83 |
|---|---|---|---|---|---|---|---|---|---|
| P-value | 0.041 | 0.035 | 0.024 | 0.027 | 0.006 | 0.061 | 0.013 | 0.006 | 0.007 |

IC location studies data

*All locations*

| Location | A1 | A2 | A3 | A4 | B1 | B2 | B3 | B4 | C1 | C2 | C3 | C4 |
|---|---|---|---|---|---|---|---|---|---|---|---|---|
| P-value | 0.212 | 0.564 | 0.523 | 0.490 | 0.045 | 0.837 | 0.407 | 0.967 | 0.080 | 0.905 | 0.638 | 0.126 |

*Locations along dimension 2 (lateral-to-medial axis)*

| Location | 1 | 2 | 3 | 4 |
|---|---|---|---|---|
| P-value | 0.001 | 0.586 | 0.232 | 0.609 |